A Study of the December 1992 Westerly Wind Burst Event during TOGA COARE

by

Chaing Chen*#, Wei-Kuo Tao*, Dean G. Duffy*,
George S. Lai*+ and Po-Hsiung Lin&

*Mesoscale Atmospheric Processes Branch
Laboratory for Atmospheres
NASA/Goddard Space Flight Center
Greenbelt, MD 20771

#Joint Center for Earth System Technology
The University of Maryland Baltimore County
Baltimore, MD 21250

+General Sciences Corporation
Beltsville, MD 20705-2675

&Dept. of Atmospheric Sciences
National Taiwan University
Taipei, Taiwan

(Submitted to Monthly Weather Review, February 1999)

Corresponding author address: Dr. Chaing Chen, Mesoscale Atmospheric Processes Branch.
NASA/GSFC, Code 912, Greenbelt, MD 20771

ABSTRACT

Using the Penn State/NCAR MM5 mesoscale model, a westerly wind burst (WWB) that occurred during the period from 19 to 30 December 1992 over the Tropical Ocean Global Atmosphere Coupled Ocean-Atmosphere Response Experiment (TOGA COARE) has been simulated and compared with observation. This event is characterized by the presence of super cloud clusters and the occurrence of a major WWB that extended over the western and central Pacific Ocean. Although several of the observed convective systems were not precisely simulated by MM5, the model did capture many other observed characteristics, such as the explosive development of convection, the cyclonic circulation and the WWB.

The WWB resulted from the coalescence of three types of tropical disturbances. The first type was a low-level westerly jet (LWJ) that developed at the equator and may be associated with the eastward propagation of an ISO (Intraseasonal Oscillation). The second type featured an easterly wave-like disturbances that originated in the south central Pacific Ocean and propagated westward. Finally, the third type involved a cross-equatorial flow that deflected Northern Hemispheric easterlies into the Southern Hemisphere and may be caused by inertial instability. These disturbances worked in concert, resulting in intense convection over the TOGA COARE region. Once intense convection developed, a large-scale cyclonic circulation was produced over the western Pacific warm pool, propagated eastward, and initiated a WWB.

1 Introduction

It has long been known (Wyrtki, 1975 and Luther *et al.*, 1983) that easterly equatorial winds in the western or mid-Pacific can abruptly reverse their direction and become westerlies often during ENSO (El Niño and Southern Oscillation). This sudden change of wind, called a westerly wind burst (WWB), may last several days, has a maximum wind speed as large as 20 m s^{-1}, and usually occurs over the region from 5 S to 5 N and from 130 E to 170 E. WWBs usually occur from November to the following May and its life-cycle is about 2 to 10 days (Keen 1987).

One possible explanation for the generation of WWBs is the eastward propagation of an ISO (Intraseasonal Oscillation) from the Indian Ocean. Lau *et al.* (1996) found that a large-scale pressure dipole with high pressure over the maritime continent[1] and low pressure over the equatorial central Pacific can form during an ISO episode. The WWB is then produced as a result of this east-west pressure gradient.

Another hypothesis suggests that cold surges from the mid-latitudes may generate equatorial westerlies (Lim and Chang 1981, Harrison 1984, Murakami and Sumathipala 1989). During TOGA-COARE, Lau *et al.* (1996) found a strong correlation between westerlies and meridional flow from the Northern to Southern Hemisphere.

The presence of quasi-stationary atmospheric heat sources over the dateline may also initiate westerlies (see Lau *et al.*, 1996). These heat sources apparently result from convection due to a positive SST anomaly (Pacific Warm Pool) over the same area. A pressure dipole resulting from the convection then produces the WWB. Lau *et al.* (1989), Sui and Lau (1992), Lin and Johnson (1996) have all shown that strong low-level westerlies usually appear near the equator after convection begins.

The purpose of this paper is two-fold. First, we will introduce a new mechanism for the generation of WWBs. In section 2, we present a conceptual model of how westwardly

[1] The maritime continent refers to the southern tip of the Indo-China (Malaysia), Indonesia (Sumatra and Borneo), and New Guinea.

propagating disturbances from the central Pacific Ocean merge with eastwardly propagating disturbances from the Indian Ocean to form a large-scale cyclonic circulations located at the dateline and just to the south of the equator. The WWB is merely the northern branch of this circulation. We then illustrate how observations confirm this model.

In the second half of this paper we examine whether the MM5 model can be used to explain the development of the WWB. In section 3, long-term integrations are made to answer this question. In section 4, a block diagram is presented to outline differences between observation and model simulation. Finally, we summarize our findings in Section 5.

2 Observed Large-Scale Features

2.1 Conceptual Representation

To understand the generation and development of the WWB, we have constructed the schematic shown in Fig. 1. In this diagram, we identify three types of tropical disturbances that interacted with each other, resulting in intense convection and a subsequent cyclonic circulation over TOGA COARE. This cyclonic circulation then moved eastward and grew in strength and size through an interaction with the Pacific warm pool. Thus, a large-scale cyclonic circulation developed and matured over the dateline, just south of the equator. The WWB is merely the westerlies along the northern (equatorial) side of this circulation.

In our conceptual model we show four distinctive stages leading to the WWB. During the initial stage, shown in Figure 1a, several disturbances are embedded in the tropics. To the east, twin cyclonic circulations (C3 and C3N) propagate westward. Meanwhile, to the west, a low-level westerly jet (LWJ) propagates eastward. In between, we have a quasi-stationary cyclonic circulation C1 in the Southern Hemisphere and a low-level easterly jet (NEJ) in the Northern Hemisphere.

The second stage (Fig. 1b) features the presence of a band of cross-equatorial flow (CEF) to the west of the cyclonic circulation C3N. This flow resulted from the inertial instability of the low-level NEJ streak over the Northern Hemisphere. As the CEF intensified, cyclonic circulation C3 propagated westward more slowly than its counterpart (C3N) in the Northern Hemisphere.

The third stage (Fig. 1c) consists of the coalescence of all three types of disturbances, i.e., LWJ, C1 and CEF. This convergence triggered convection and the subsequent genesis of the cyclonic circulation C5.

The fourth stage (Fig. 1d) shows the mature stage of cyclonic circulation C5. The WWB is the westerlies that develop along the equatorial side of C5. Also, during this stage, cyclonic circulation C3N vanishes. In its place, a prominent band of CEF develops which

subsequently recurves the Northern Hemispheric easterlies into cyclonic circulation C5.

Having introduced this overview of the evolution of a WWB, we now elaborate each stage with a detailed synoptic analysis. In the following, the datasets are from NCEP's (National Centers for Environmental Prediction) global analyses archived at NCAR (National Center for Atmosphere Research) at a 2.5° latitude/longitude resolution. To show the relationship between convection and tropical disturbances, GMS Tbb (black body-like temperature) datasets were used.

2.2 Nascent Stage (from 13 to 19 December 1992)

The nascent stage is characterized by the presence of several wave disturbances that developed over 140 E - 140 W and 5 N - 30 S. These disturbances propagated westward from the central Pacific Ocean or eastward from the Indian Ocean. Each disturbance played its particular role in the generation of intense convection and the subsequent development of the WWB.

Using 850 mb vorticity and streamlines analyses, Fig. 2 shows the westwardly propagating disturbances. For the purpose of tracking, we use boxes, tagged with numbers, to indicate the location and identity of these disturbances. Only disturbances that are important in understanding the generation of the WWB event are highlighted.

During this stage, as shown in Figs. 2a-2c, the cyclonic disturbance labeled by C1[2] meandered in the vicinity of 160 E. Meanwhile, disturbance C2, a mid-latitude system now located at latitudes 20-30 S, propagated eastward. On the other hand, cyclonic disturbances C3 and C4 propagated westward. Toward the end of this stage (Fig. 2c), disturbances C2, C3, and C4 converged. Although the origin of cyclonic disturbances C3 and C4 is beyond the scope of this study, these disturbances appear to originate over the central Pacific Ocean and they propagated in the manner of an easterly wave.

Longitude-time analyses of vorticity averaged between 17 S to 12 S, were useful in detect-

[2]We drop the prefix "C" in the figures.

ing the presence of westwardly propagating disturbances. The disturbance associated with the upper line in Fig. 3 is the cyclonic disturbance C4 shown in Fig. 2. The bottom line is associated with another cyclonic disturbance that plays no role in our study; it is merely one of many westwardly propagating cyclonic disturbances encountered in the tropics.

The presence of westwardly propagating cyclonic disturbances is also confirmed in the longitude-time analyses of the GMS Tbb dataset (see Fig. 4). In this figure[3], we superimposed the same solid lines that were plotted in Fig. 3. These lines show that the observed convective systems were indeed connected with westwardly propagating cyclonic disturbances. Figure 4 also shows that intense convection began after 25 December near 170 E and appears to be associated with the arrival of these disturbances from eastern longitudes. On the other hand, the main convective system associated with the eastwardly propagating ISO from the Indian Ocean stalled near 140 E. Therefore, our results are an exception to the conventional ISO paradigm. The reason for these differences may lie with the fact that our latitudinal band is averaged away from the equator. Because Kelvin waves decay rapidly away from the equator, Fig. 4 may not include eastwardly propagating Kelvin waves. For this reason, we performed additional analyses where the latitudinal averaging band is closer to the equator (0-7 S). When this was done, two eastwardly propagating signals (L1, L2) began to emerge (see Fig. 5). These signals can be traced back to the Indian Ocean. Of the two, the L2 signal is probably an eastwardly propagating ISO disturbance (Chen *et al.* 1996).

In addition to these eastwardly propagating signals, we can also identify westwardly propagating signals (M1 – M4) in Fig. 5. M4 is the cyclonic disturbance C3 shown in Fig. 2. The coalescence of the eastwardly (L2) and westwardly (M2, M3 and M4) propagating disturbances appears to play an important role in producing intense convection after 20 December 1992 near 160 E.

In Fig. 6, we highlight the eastwardly propagating disturbance by streamline and zonal velocity (u) analyses. There is a streak of low-level westerlies (LWJ) propagating in the

[3]Figure 4 has a different longitudinal domain coverage from that in Fig. 3.

vicinity of the equator over the western Pacific with a speed of approximately of 3-4 m s^{-1}. This LWJ may be associated with the L2 disturbance shown in Fig. 5. There is also an easterly jet (NEJ) streak located over 10 N and 170 E (see Fig. 6a). This NEJ appears to play an important role in triggering inertial instability that produced the cross-equatorial flow (CEF) shown in Fig. 6c.

2.3 CEF Developing Stage (from 19 to 21 December 1992)

This stage is characterized by the development of cross-equatorial flow. In Fig. 7, the vorticity and streamline analyses show that cyclonic disturbances C3 and C3N propagated westward over the Southern and Northern Hemispheres, respectively. Because of their symmetric structure with respect to the equator on 16 December (see Fig. 7a), we suggest that they are westwardly propagating Rossby-gravity waves, forming a so-called "cross-equatorial cyclone pair" (Keen 1982). However, this symmetric structure disappeared approximately five days later. On 21 December (not shown), C3N had propagated faster than its counterpart C3 over the Southern Hemisphere. Simultaneously, a band of northerly CEF developed to the west of cyclonic disturbance C3N. The generation of this band of CEF is mostly likely due to inertial instability, because the flow over 160-170 E and 0-5 S was inertially unstable due to the presence of positive absolute vorticity over this region (see Fig. 7a). Past studies (Dunkerton 1993, Stevens 1983, Tomas and Webster 1997) have showed that zonal shear flows near the equator can trigger inertial instability and produce CEF if $f(f + \zeta) < 0$, where f is the Coriolis parameter and ζ is the relative vorticity. If we take the jet's zonal velocity to be 10 m s^{-1} and its half-width to be 1000 km (see Fig. 6a) and assume that the curvature of the jet profile is small, the e-folding time for the instability is approximately 2.3 days (Stevens 1983). This is consistent with the observed growth rate of our CEF.

2.4 Disturbances Coalescencing Stage (from 21 to 25 December 1992)

The coalescence of cyclonic disturbance C1, an eastwardly propagating LWJ jet streak and a band of CEF over the TOGA COARE region is the most significant event during this stage. Using all possible sources of data, Fig. 8 shows the large-scale environment during the development of intense convection near TOGA COARE (150-160 E and 0-10 S). We have superimposed GMS Tbb upon the streamlines to illustrate the relationship between the development of convection and the propagation of disturbances. Again, we use boxes (westwardly moving and associated with cyclonic disturbances) and circles (eastwardly moving and associated with the LWJ) to track the location of these disturbances.[4]

In summary, cyclonic disturbance C1 stalled around 170-160 E. To the east of this region a cyclonic disturbance C3 propagates westward toward C1. To the west, a LWJ propagates eastward toward C1. Simultaneously, cyclonic disturbance C3N propagates westward in the Northern Hemisphere associated with a band of CEF. By 22 December (Fig. 8c), when the LWJ, the band of CEF and the cyclonic disturbance C1 begin to coalesce or merge, intense convection occurs over the region near TOGA COARE.

2.5 Maturing Stage (after 25 December 1992)

During this stage the WWB develops over the equatorial western Pacific Ocean. This stage begins with the generation of a large-scale cyclonic circulation (C5), commonly called the Rossby gyre (Chen *et al.* 1996), on 25 December (Fig. 9a) between 155 - 170 E and 15 - 0 S. Following Gill (1980), we suggest that the latent heat release over TOGA COARE after 22 December (Fig. 7c) is the primary reason for this cyclonic circulation.

On 27 December (Fig. 9b), C5 moves southeastward and develops explosively due to intense convection. Simultaneously, an enhanced CEF develops. By 29 December (Fig. 9c), this cyclonic disturbance has grown to cover a large area (160 – 180 E and 5 20 S).

[4]The location of these symbols is the same as that in Fig. 7

In general, this large-scale cyclonic circulation propagates in a southeastwardly direction toward the western Pacific warm pool (see Fig.10). Throughout the entire mature stage, strengthening of the cyclonic circulation occurs because the warmer SST's induces intense convection.

During this stage, a positive relationship exists between the intensification of the WWB and the development of the large-scale cyclonic disturbance. Low-level streamlines and zonal flow analyses (Fig. 11) show that the presence of the WWB corresponds to the westerlies that develop along the equatorial side of C5. The mature development of C5 coincides with the maximum intensity of the WWB.

3 Model simulations

In the previous section, we described the observed evolution of a WWB. In this section, we show the results from MM5 model simulations. Our motivations are two-fold: Can MM5 reproduce the observed features? Can we use the model to explore the mechanisms responsible for the intensification of convection, the subsequent development of the observed large-scale cyclonic circulation and the resulting WWB?

3.1 Model

In brief, MM5 (Dudhia 1993) is a three-dimensional, nonhydrostatic mesoscale model with a terrain-following coordinate. It uses finite differences and a time-splitting scheme to solve prognostic equations on a Arakawa type-B staggered grid. MM5 employs observed wind, temperature and humidity as its initial condition and incorporates realistic topography and sophisticated physical processes to represent the appropriate forcings. These physical processes include clouds, a planetary boundary layer (PBL), long- and short-wave radiation, and surface fluxes of heat, moisture and momentum. Because of the wide variety of physical parameterizations that can be used in MM5, only an overview of those that are relevant are listed below:

1. The model was initialized from NCEP's archived analyses. The time-varying, lateral boundary conditions were provided at 12-h intervals. The model was integrated from 0000 UTC 19 December to 0000 UTC 31 December 1992.

2. Two nested domains were constructed with a grid resolution of 135 and 45 km, respectively; the corresponding numbers of grid points in (x, y, σ) are 151 $\times$ 73 $\times$ 23 and 133 $\times$ 259 $\times$ 23. The model top is located at 50 hPa level. A time step of 180 and 60 s are used in the coarse and inner nested grids, respectively.

3. The Betts-Miller parameterization scheme (Betts 1986, Betts and Miller 1986, Betts

and Miller 1993) was used. This scheme was designed to represent the quasi-equilibrium state established by convection. Latent heat is released as the sounding relaxes toward a reference profile over a given period of time. This reference profile is consistent with the observed post-convective environment.

4. A three-class cloud microphysics scheme (Dudhia 1989) is used for the resolvable scale convection. This scheme allows for ice-phase processes: Cloud water becomes cloud ice and rain water becomes snow when the temperature is below the freezing point.

5. The atmospheric radiation model includes long-wave (infra-red) and short-wave (visible) parameterizations that interact with the atmosphere (Dudhia 1989). This scheme uses broad band and a two-stream (upward and downward fluxes) approach for the radiative flux calculation. It also allows for ice, precipitation and carbon dioxide effects in the long-wave scheme.

3.2 Conceptual Representation

In general, the model simulation reproduced cyclonic disturbance C5 near TOGA COARE. Later on, C5 grew to become a large-scale cyclonic circulation near the dateline. Both the temporal and spatial aspects of our simulated large-scale cyclonic circulation agree well with observation.

In spite of an overall good agreement with observation, there were several notable differences. These differences were caused by the lack of any initially organized convective system. Because our model uses a finer resolution (45 km) than NCEP's global model and is not initialized with convection, it requires a spinup time to readjust and produce convection. Despite these differences, we were still able to capture the evolution of the system over TOGA COARE during the December 1992 WWB. In the following, we highlight the similarities and differences between the simulation and observation.

The initial stage shown in Fig. 12a is identical to that shown in Fig. 1a. However, by

the second stage (Fig. 12b) differences appear between the simulation and observation (Fig. 1b). For example, during the development of the CEF, C1 moved eastward rather than remaining stationary, resulting in a weaker CEF that contained northwesterlies.

The third stage is shown in Fig. 12c. Unlike our observational findings, C1 continued to move eastward as LWJ and CEF began to interact with each other with a simultaneous genesis of cyclonic disturbance C5. Despite these differences, by the fourth stage (Fig. 12d) the numerical simulation agreed with observation (Fig. 1d) except that there is a weaker C1 orbiting together with C3 along the outer periphery of the large-scale cyclonic circulation C5. Although the main characteristics of C1 were not reproduced well by the simulation, the evolution of C5 agreed well with observation. The model simulation showed that the generation of C5 depended on on barotropic instability, not just C1.

With this overview of our results, we now present detailed results from five particular events: (1) the development of CEF, (2) the role of LWJ, (3) the development of convection, (4) the generation of cyclonic disturbance C5 and (5) the generation of the WWB. Because the model was initialized at 0000 UTC 19 December 1992, its initial conditions contained all of the nascent disturbances.

3.3 The Development of CEF

The simulated CEF differed from observation: After the northerly CEF passed over the equator, its wind direction became westerly over an area to the west of C1a (see Figs. 13b-c) while the observed CEF retained its northerly wind component until it reached TOGA COARE. The reason for these differences lies in the evolution of the cyclonic disturbance C1. The model simulation shows that C1 propagated eastward while observation shows that C1 is quasi-stationary.

Why did C1 evolve differently? One possible reason may be the fact that the model does not initialize clouds. Another possibility may lie in the higher resolution used in our simulation. For example, in the vorticity and streamlines analyses (Fig. 13), we note the

presence of many small features. After one day of simulation (22 December, Fig. 13b), cyclonic disturbances C1 and C3 disintegrated into several pieces and formed four vorticity centers (C1a, C1b, C3a and C3b). This breakdown of vorticity ribbons into vorticity centers, similar to that shown in Figs. 13a and 13b, has been studied by many investigators (Kuo and Hong 1994, Smyth and Peltier 1994, Wirth *et al.* 1997) and occurs due to the mutual intensification of counter-propagating Rossby waves across the vorticity strip (Hoskins *et al.* 1985). After the breakdown, as can be seen in Figs. 13b and 13c, cyclonic disturbances C1a and C1b moved eastward. Simultaneously, cyclonic disturbance C5 began to develop over TOGA COARE. Eventually, C5 (see Figs. 13d-f) evolved into a large-scale cyclonic circulation near the dateline.

3.4 The role of LWJ

By examining Fig. 14's streamlines and zonal flow, we find that the eastward propagation of C1a and C1b (see Figs. 13b-d) coincides with the eastward propagation of the LWJ. This differs from observation. Furthermore, two LWJ (Figs. 14a-14c, circles connecting by lines) developed in the model simulation. The right LWJ appears to be responsible for the eastward propagation of C1a and C1b, while the left one generates disturbances C5. Subsequently, the low-level westerlies intensified at later times along the northern (equatorial) side of C5 (see Figs. 14d-f) and exhibited a WWB.

3.5 The development of convection

If we superimpose the location of cyclonic disturbances (Fig. 13), LWJ (Fig. 14) and predicted precipitation shown in Fig. 15, we can reach two conclusions. Firstly, flow convergence can produce convection. Secondly, intense convection can result in the development of cyclonic circulations. For example, one day into the simulation (Fig. 15a), the model produced two cloud bands (double ITCZs) along the northern and southern sides of the equator in a region to the east of 160 E due to the convergence of northeasterlies and southeasterlies

in the Northern and Southern Hemispheres, respectively. Another example is the generation of a wedge-like cloud band structure (Fig. 15b) when C1a, CEF and LWJ coalesced in the area near 155 – 165 E and 0 - 5 S. This wedge consisted of a protruding point at the leading edge of the right LWJ and two cloud bands along the sides. The northern cloud band was generated by the convergence of the westerlies with the northerly CEF; the southern cloud band was produced by the interaction with C1a.

Once convection developed, we found that the latent heat release induced cyclonic circulations as predicted by Gill (1980). Furthermore, intense convection appeared to play an important role in the matured development of C5 (Figs. 15d-f)

3.6 The Generation of Cyclonic Disturbance C5

The mechanism that generated cyclonic disturbance C5 in the model simulation differs from observation. As previously discussed, observations showed that northerlies from the CEF, westerlies from the LWJ and southerlies from C1 converged over TOGA COARE, triggering intense convection. Latent heat release resulted in the generation of C5.

The model simulation shows however that the convergence of LWJ, CEF and C1 was not important in producing intense convection over TOGA COARE because C1 is no longer quasi-stationary. A possible mechanism for the excitation of C5 may be barotropic instability associated with the presence of the LWJ. The simulated growth rate of C5 is approximately 1-2 days. This time scale is consistent with the theoretical growth rate for barotropic instability. If we assume that the meridional wind shear of the LWJ is 10 m s^{-1} per 300 km so that the relative vorticity (ζ) is 3.3×10^{-5} s^{-1}, then the e-folding time is approximately 1.4 days ($4/\zeta$, Kuo and Horng 1994).

3.7 The Generation of WWB

Although our model simulations differed from observation on the origin of the cyclonic disturbance C5, there was good agreement with observation regarding the mature stage of

C5 and the generation of WWB. As shown in Figs. 13b and 13c, C5 initially formed on 22 December near TOGA COARE. It grew rapidly, became a major cyclonic system within 1-2 days (24 December) and then moved eastward during the following three days (25-27 December, Figs. 13d-13e). Finally, this disturbance moved in a southeastward direction, before becoming the center of a large-scale cyclonic circulation (Fig. 13f). The simulated C5 tracked in a similar manner as the observation.

Although the model generated two LWJs (Figs. 14a-14c), the evolution of the WWB agrees with observation. For example, the rapid intensification of the second (left) LWJ on 24 December (see Fig. 14c) can be regarded as the first sign of the WWB. Observation (Fig. 11) also showed a similar beginning. Furthermore, during the following days (25-29 December, Figs. 14d-f), westerlies strengthen in the same manner as did C5. Consequently, when this cyclonic disturbance moved southeastward to become a large-scale cyclonic circulation, the corresponding westerlies also expanded eastward, covering the equatorial southern Pacific Ocean from 155 E to 175 E. All of these characteristics are consistent with observation.

In the previous section, we suggested that the WWB is the manifestation of westerlies that occur on the equatorial side of the cyclonic circulation. Results from the model simulation confirm that the WWB is indeed closely related to the presence of large-scale cyclonic circulations that develop near the equator at the dateline.

4 Discussion and Future Study

We have shown that interactions between an eastwardly propagating LWJ and several westwardly propagating tropical cyclonic disturbances can generate a large-scale cyclonic circulation and WWB. In this section, we use a block diagram (Fig. 16) to highlight those processes that create the WWB. We also use this diagram to introduce conjectures that remain to be tested.

In Fig. 16, we show that the WWB resulted from the generation of a large-scale cyclonic circulation which has its origin in the convectively intensified C5. Along with this large-scale cyclonic circulation, an enhanced CEF also developed. The generation of such a prominent CEF is not unusual. In her study of synoptic settings of WWBs based on 10 years of data, Hartten (1996) showed that CEFs which move from the Northern Hemispheric easterlies into the Southern Hemispheric westerlies are a prominent feature during the months December to February.

If we trace this block diagram backwards, observation shows that the generation of C5 resulted from convection. This finding is consistent with Gill's (1980) work. He showed that a constant, stationary heat source in a tropical atmosphere can produce cyclonic circulations. The coalescence of the LWJ with the CEF and C1 resulted in intense convection.

As shown by model simulation, barotropic instability may well have played as important a role as latent heat release in producing C5. The initial vorticity center associated with the arrival of the LWJ over TOGA COARE grew at a rate of 1-2 days, which is consistent with the theoretical growth rate of 1.4 days for the observed meridional wind shear of the LWJ.

To complete the block diagram, we also show that the LWJ was associated with an eastwardly propagating Kelvin wave, while C1, C3 and C3N are associated with Rossby-gravity waves. Furthermore, we suggest that the CEF resulted from inertial instability.

Our study raises further questions concerning WWBs. These questions include how inertial instability leads to the development of the CEF and how CEFs interact with the

LWJ to produce cyclonic disturbances. Although we did not address the origin of the LWJ, we suggest that it is a part of the ISO signal that propagates eastward from the Indian Ocean. A future study should focus on what role does the western Pacific and the eastern Indian Oceans play in the relationship between the LWJ and the ISO.

5 Summary

By conducting data analyses and MM5 model simulations, we have studied a westerly wind burst that occurred between 19 and 30 December 1992. This WWB was associated with the generation and the intensification of a large-scale cyclonic circulation in the Southern Hemisphere over 160 – 180 E and 5 – 20 S; westerly flow developed along the equatorial side of the cyclonic circulation. Although the exact timing and location of several observed convective systems were not well simulated by MM5 (as expected), the model did capture many other observed features, such as the explosive development of intense convection, the cyclonic circulation and the WWB.

Convection played an important role in the generation of the cyclonic circulation and the subsequent development of the WWB. As explained by Gill (1980), latent heat release in the tropical atmosphere can produce such a circulation. Lin and Johnson (1996) also reached a similar conclusion in their study of flow characteristics during TOGA COARE.

Low-level convergence associated with the large-scale flow was an important factor in generating convection. This convergence over TOGA COARE resulted from the coalescence of a LWJ (moving eastward) and a Rossby-gravity wave disturbance (moving westward). Additional convergence was furnished by an intensifying CEF due to the inertial instability of an easterly jet located near 10 N and 160-170 E.

Although we have suggested that convection is important in generating large-scale cyclonic circulations, barotropic instability may also be another important mechanism. In our numerical study, a LWJ triggers barotropic instability over TOGA COARE.

The large-scale gyre in this study had a complex structure. It consisted primarily of a vortex at its center and several vortexes pinwheeling in a clockwise direction along the eastern circumference of the large-scale cyclonic circulation. The radius of the gyre was about 1000 km.

The principal finding of this study is the realization that westwardly propagating cyclonic

disturbances that originate over the central Pacific Ocean and a band of CEF can play an important role in the generation of convective and cyclonic systems over the western Pacific Ocean. According to the classical ISO paradigm, wave disturbances always develop over the Indian Ocean and move eastward; westwardly moving cyclonic disturbances and the CEF play no role at all. However, our findings indicate otherwise. Because of our findings, an expanded view of the origin of tropical disturbance may be needed.

Acknowledgments.

Dr. S. S. Chen is thanked for her suggestions during the course of the study. Drs. R. Kakar and R. Adler are thanked for their support of this research. Additional acknowledgement is made to NASA/GSFC for computer resources used in the research.

6 References

Betts, A. K., 1986: A new convective adjustment scheme. Part I: Observational and theoretical basis. *Quart. J. Roy. Meteor. Soc.*, **112**, 677–691.

_____, and M. J. Miller, 1986: A new convective adjustment scheme. Part II: Single column tests using GATE wave, BOMEX, ATEX and Arctic air-mass data sets. *Quart. J. Roy. Meteor. Soc.*, **112**, 693–709.

_____, and _____, 1993: The Betts-Miller scheme. The representation of cumulus convection in numerical models. K. A. Emanuel and D. J. Raymond, Eds., Amer. Meteor. Soc., 246pp.

Chen, S. S., R. A. Houze, Jr., and B. E. Mapes, 1996: Multiscale variability of deep convection in relation to large-scale circulation in TOGA COARE. *J. Atmos. Sci.*, **53**, 1380–1408.

Dudhia, J., 1989: Numerical study of convection observed during the winter monsoon experiment using a mesoscale two-dimensional model. *J. Atmos. Sci.*, **46**, 3077–3107.

_____, 1993: A nonhydrostatic version of the Penn State-NCAR mesoscale model: Validation tests and simulation of an Atlantic cyclone and cold front. *Mon. Wea. Rev.*, **121**, 1493–1513.

Dunkerton, T. J., 1993: Inertial instability of nonparallel flow on an equatorial β plane. *J. Atmos. Sci.*, **50**, 2744–2758.

Gill, A. E., 1980: Some simple solutions for heat-induced tropical circulation. *Quart. J. Roy. Meteor. Soc.*, **106**, 447–462.

Harrison, D. E., 1984: The appearance of sustained equatorial surface westerlies during the 1982 Pacific warm event. *Science*, **224**, 1099–1102.

Hartten, L. M., 1996: Synoptic settings of westerly wind bursts. *J. Geophys. Res.*, **101(D12)**, 16, 997–17,019.

Hoskins, B. J., M. E. McIntyre, and A. W. Robertson, 1985: On the use and significance of isentropic potential vorticity maps. *Quart. J. Roy. Meteor. Soc.*, **111**, 877–946.

Keen, R. A., 1982: The role of cross-equatorial tropical cyclone pair in the Southern Oscillation. *Mon. Wea. Rev.*, **110**, 1405–1416.

_____, 1987: Equatorial westerlies and southern oscillation. Proc. of the US TOGA Western Pacific Air-Sea Interaction Workshop. R. Lukas and P. Webster, Eds., Honolulu, 121 140.

Kuo, H.-C., and C.-H. Horng, 1994: A study of finite amplitude barotropic instability. *Terrestrial, Atmospheric and Oceanic Sci.*, **5**, 199 243.

Lau, K.-M., L. Peng, C.-H. Sui, and T. Nakazawa, 1989: Dynamics of super cloud clusters, westerly wind burst, 30-60 day oscillations and ENSO: An unified view. *J. Meteor. Soc. Japan*, **67**, 205–219.

_____, P. J. Sheu, S. Schubert, D. Ledvina, and H. Weng, 1996: Evolution of large-scale circulation during TOGA COARE: Model intercomparison and basic features. *J. Clim.*, **9**, 986–1003.

Lim, H., and C. P. Chang, 1981: A theory for midlatitude forcing of tropical motions during winter monsoon. *J. Atmos. Sci.*, **38**, 2377–2392.

Lin, X., and R. H. Johnson, 1996: Kinematic and thermodynamic characteristics of the flow over the western Pacific warm pool during TOGA COARE. *J. Atmos. Sci.*, **53**, 695–715.

Luther, D. S., D. E. Harrison, and R. Knox, 1983: Zonal winds in the central equatorial Pacific and the onset of El Niño. *Science*, **222**, 327 330.

Murakami, T., and W. L. Sumathipala, 1989: Westerly bursts during the 1982/83 ENSO, *J. Clim.*, **2**, 71–85.

Smyth, W.D., and W.R. Peltier, 1994: Three-dimensionalization of barotropic vortices on the f- plane. *J. Fluid Mech.*, **265**, 25–64.

Stevens, D. E., 1983: On symmetric stability and instability of zonal mean flows near the equator. *J. Atmos. Sci.*, **40**, 882–893.

Sui, C.-H., and K.-M. Lau, 1992: Multiscale phenomena in the tropical atmosphere over the western Pacific. *Mon. Wea. Rev.*, **120**, 407–430.

Tomas, R. A., and P. J. Webster, 1997: The role of inertial instability in determining the location and strength of near-equatorial convection. *Quart. J. Roy. Meteor. Soc.*, **123**, 1445-1482.

Wirth, V., C. Appenzeller, and M. Juckes, 1997: Signatures of induced vertical air motion accompanying quasi-horizontal roll-up of stratospheric intrusions. *Mon. Wea. Rev.*, **125**, 2504–2519.

Wyrtki, K., 1975: Fluctuations in the dynamic topography in the Pacific Ocean. *J. Phys. Oceanogr.*, **5**, 450–459.

FIGURE CAPTIONS

FIG. 1 Schematic diagram based on observations showing the generation of a large-scale gyre during its (a) beginning, (b) triggering, (c) developing and (d) maturing stages. The westerly wind packet is denoted by LWJ. The cyclonic circulations labeled with numbers (C3, C3N) represent eastwardly propagating Rossby waves. The circulation C1 is quasi-stationary. The resulting large-scale gyre is labeled by C5. The shaded area represent the convergence zone.

FIG. 2 The $z = 1$ km vorticity (shaded, in units of 10^{-5} s^{-1}) and streamline analyses at 0000 UTC on (a) 13, (b) 15 and (c) 19 December 1992. Boxes trace the propagation of disturbances. At the top of the box, we use a number to label different disturbances.

FIG. 3 Longitude-time Hovmöller diagram showing the vorticity (shaded, in unites of 10^{-5} s^{-1}) averaged between 12- 17 S. Lines trace the westward propagation of disturbances.

FIG. 4 Same as in Fig. 3, except for GMS Tbb and different longitudinal coverage. The lines from Fig. 3 are redrawn on Fig. 4.

FIG. 5 Same as in Fig. 4, except that the GMS Tbb is averaged between 0- 7 S. The lines denoted by L1 and L2 represent disturbances that propagated eastward, while the lines denoted by M1 – M4 represent disturbances that propagated westward.

FIG. 6 The $z = 1$ km streamline and zonal velocity (shaded, in units of m s^{-1}) analyses at 0000 UTC on (a) 16, (b) 19 and (c) 22 December 1992. Circles trace the propagation of the LWJ. The connecting solid line shows the eastward propagation of the wave. A box is used to denote the NEJ which is located over 150- 170 E and 5–10 N on 16 December 1992.

FIG. 7 Same as in Fig. 6, except for vorticity (shaded, in units of 10^{-5} s^{-1}) and streamline analyses. We superimpose boxes and circles to show the location of the westwardly propagating Rossby wave and the eastward propagation of the LWJ, respectively.

FIG. 8 Same as in Fig. 7, except for the GMS Tbb (shaded, in units of ^{0} K) analyses.

FIG. 9 Same as in Fig. 8, except for 0000 UTC on (a) 25, (b) 27 and (c) 29 December 1992.

FIG. 10 Surface temperature (shaded, in units of ^{0} C) analyses at 0000 UTC, 19 December 1992.

FIG. 11 Same as in Fig. 6, except for 0000 UTC on (a) 25, (b) 27 and (c) 29 December 1992.

FIG. 12 Same as in Fig. 1, except the diagram is based on the model simulation.

FIG. 13 The $z = 1$ vorticity (shaded, in units of 10^{-5} s^{-1}) and streamline analyses of the control case at 0000 UTC on (a) 20, (b) 22, (c) 24, (d) 25, (e) 27 and (f) 29 December 1992. Boxes with labels identify the location of disturbances in this study.

FIG. 14 Same as in Fig. 13, except for the zonal flow velocity (shaded, in units of m s^{-1}) analyses. The connecting solid lines show the eastward propagation of westerly wind packets.

FIG. 15 Same as in Fig. 13, except for the model simulated rain rate (shaded, in units of mm hr^{-1}). Boxes and circles show the location of the westwardly propagating Rossby wave and the eastwardly propagating LWJ, respectively.

FIG. 16 Block diagram showing processes that can lead to the generation of a WWB.

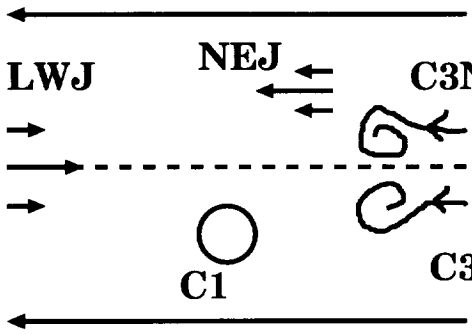

(a)

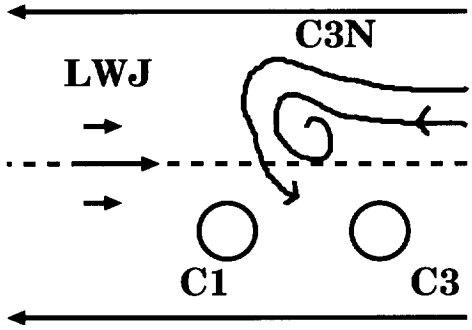

(b)

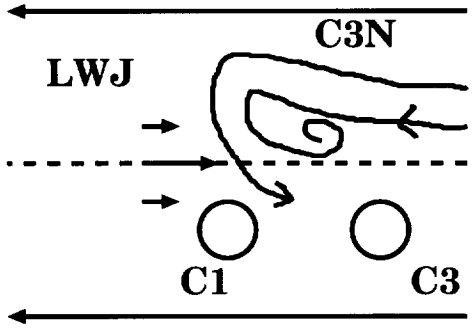

(c)

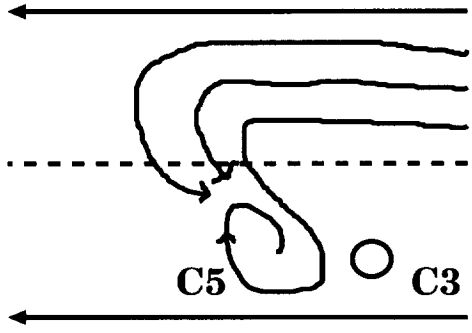

(d)

F-91

Z = 1 km Vorticity & Streamlines

0000 UTC 13 DEC 1992

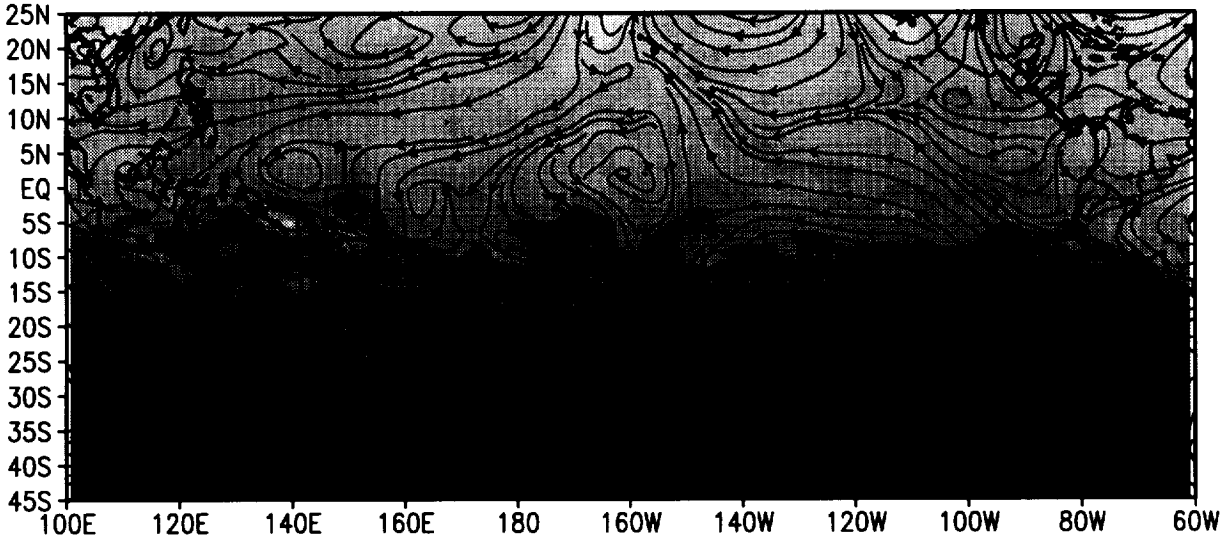

0000 UTC 15 DEC 1992

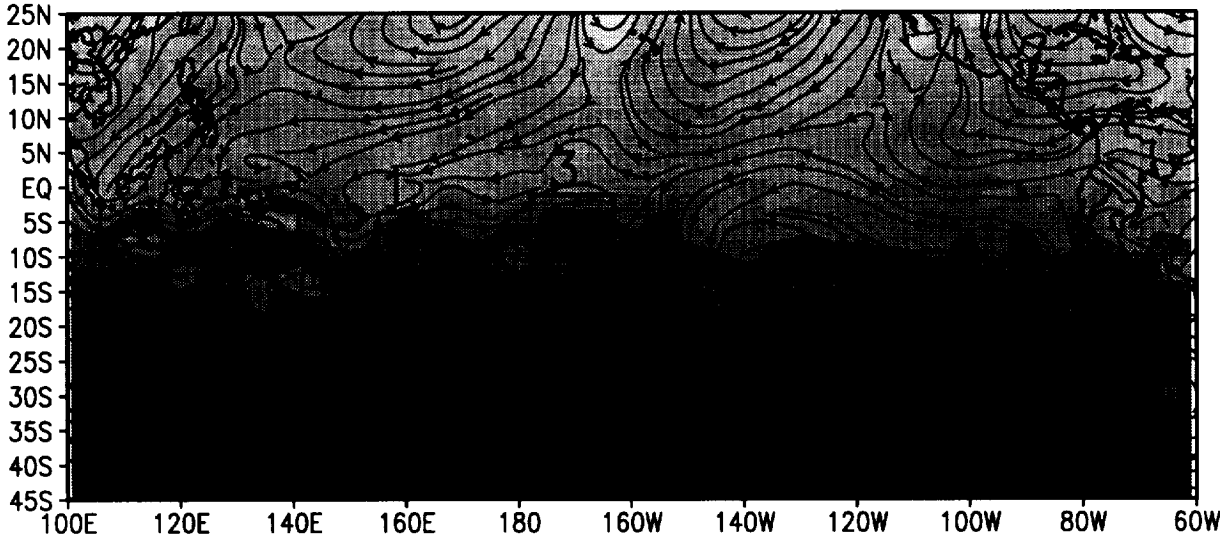

0000 UTC 19 DEC 1992

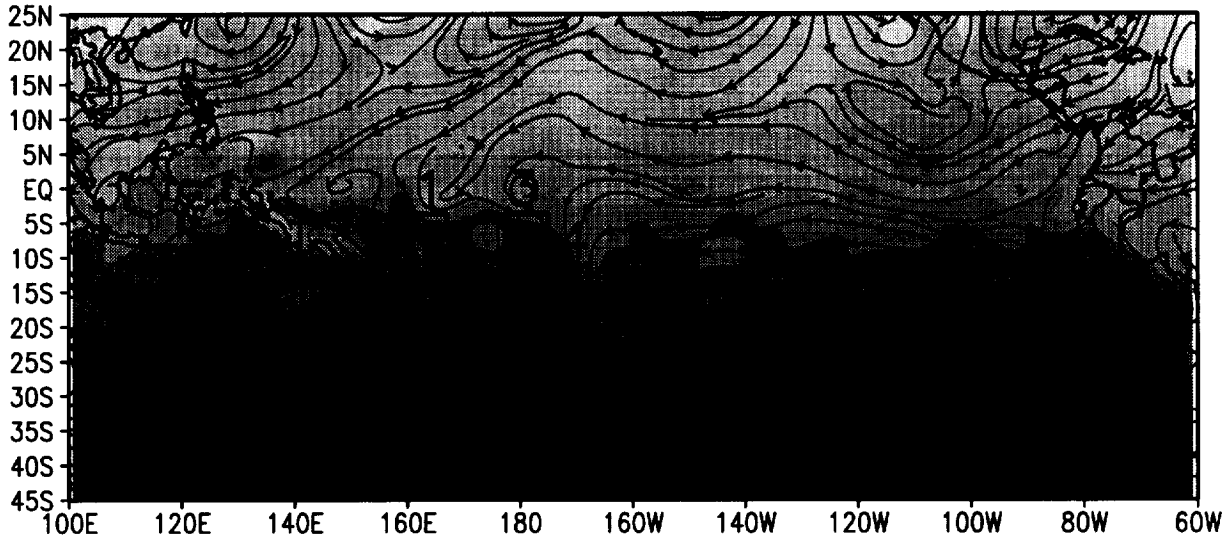

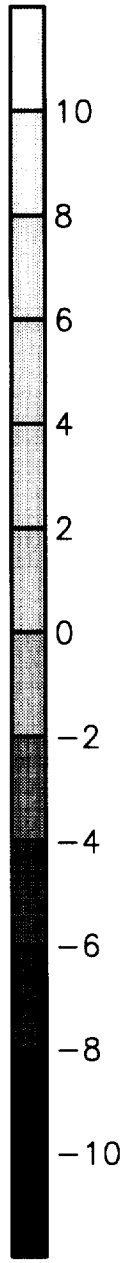

Fig 2

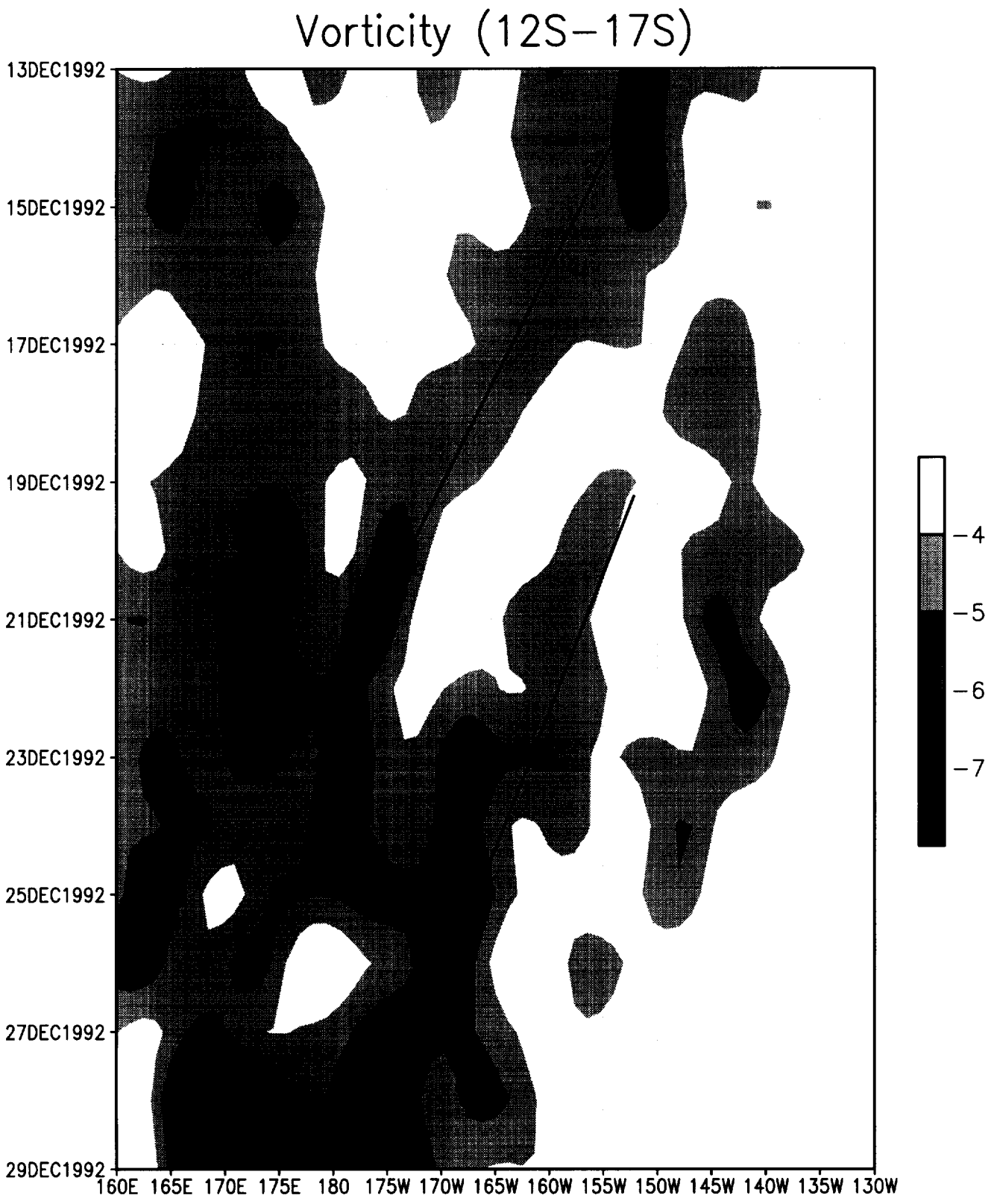
Vorticity (12S–17S)
13DEC1992
15DEC1992
17DEC1992
19DEC1992
21DEC1992
23DEC1992
25DEC1992
27DEC1992
29DEC1992
160E 165E 170E 175E 180 175W 170W 165W 160W 155W 150W 145W 140W 135W 130W
−4
−5
−6
−7

Fig 3

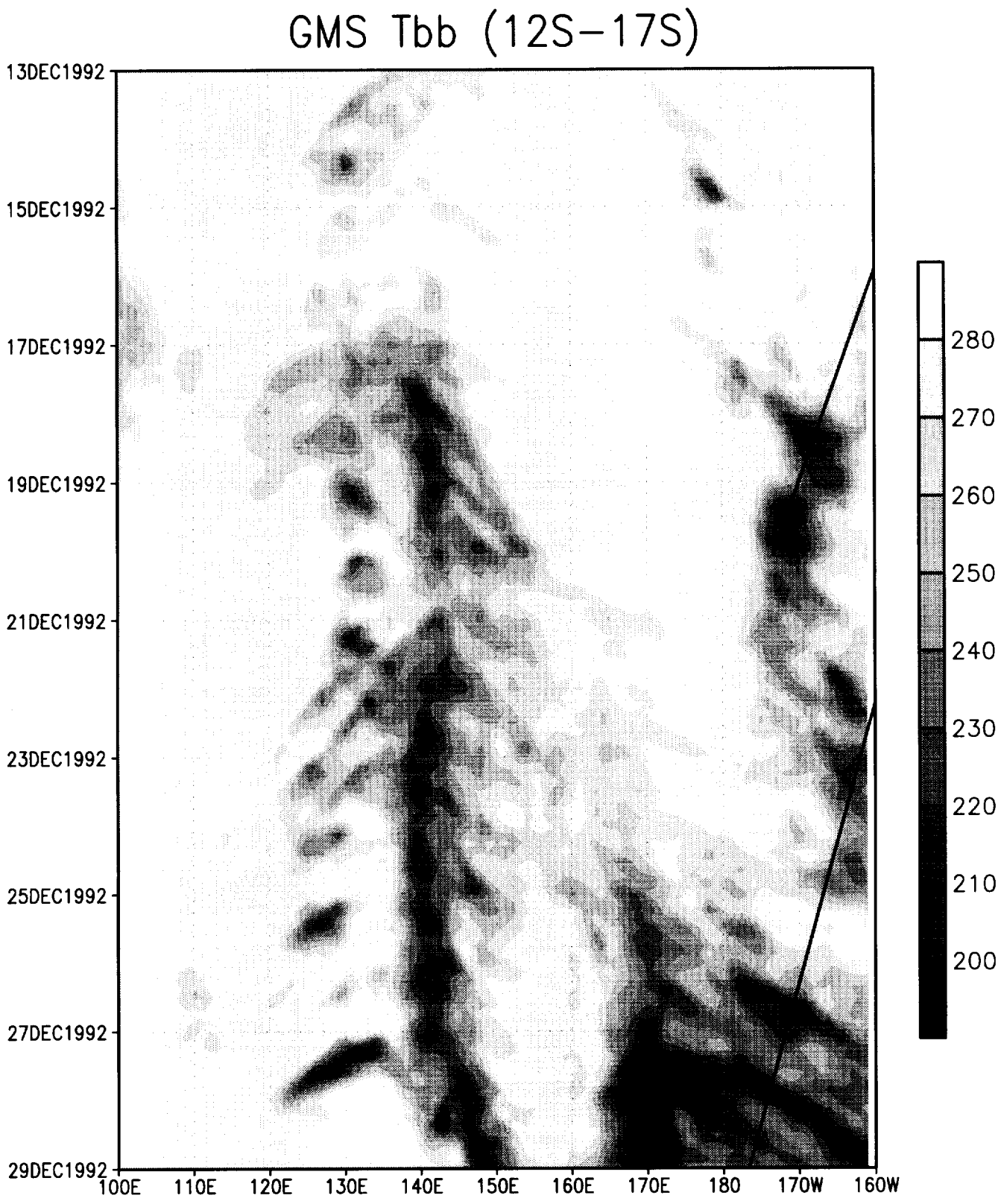
GMS Tbb (12S–17S)
13DEC1992
15DEC1992
17DEC1992
19DEC1992
21DEC1992
23DEC1992
25DEC1992
27DEC1992
29DEC1992
100E
110E
120E
130E
140E
150E
160E
170E
180
170W
160W
280
270
260
250
240
230
220
210
200

Fig 4

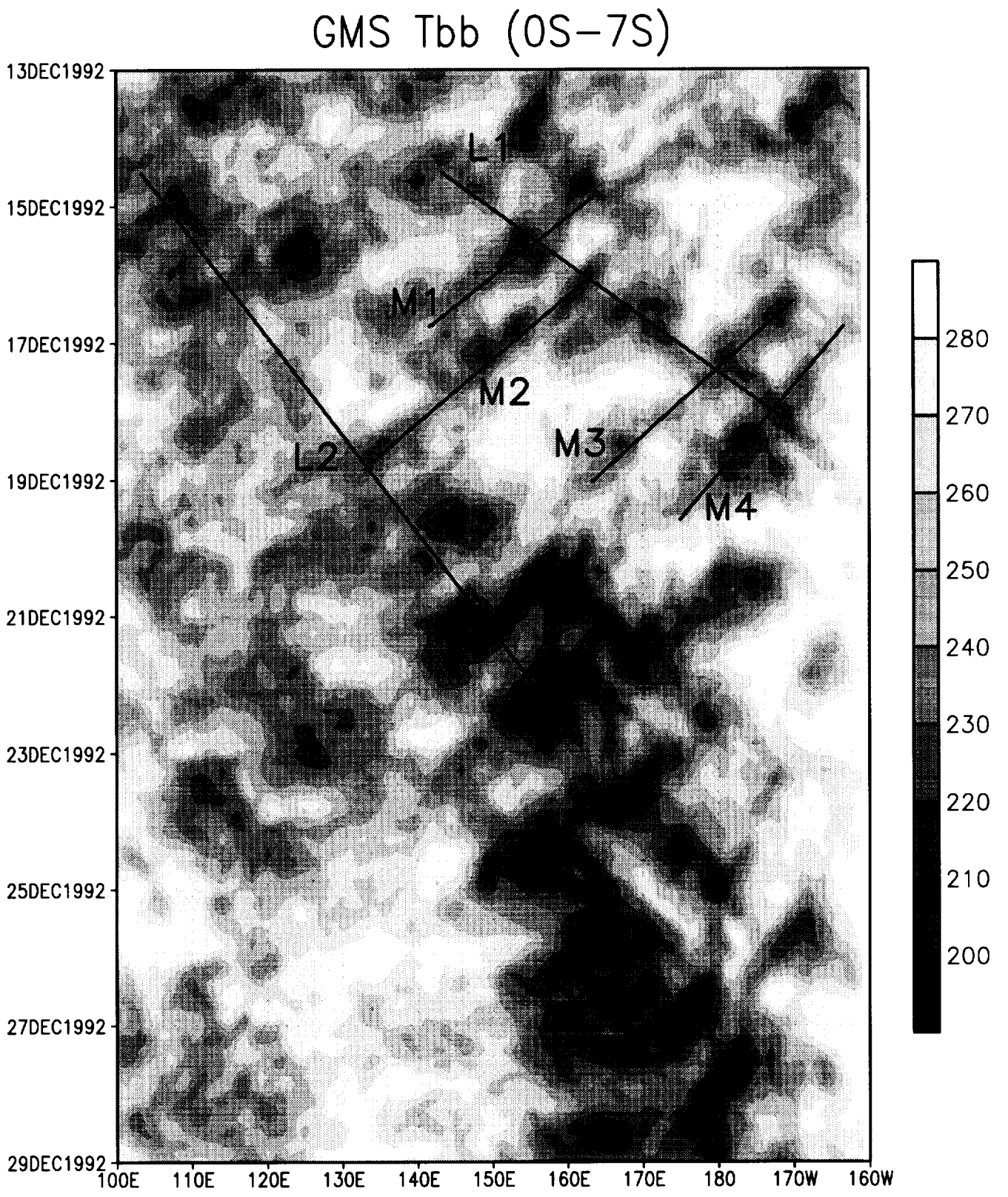
GMS Tbb (0S-7S)
13DEC1992
15DEC1992
17DEC1992
19DEC1992
21DEC1992
23DEC1992
25DEC1992
27DEC1992
29DEC1992
100E
110E
120E
130E
140E
150E
160E
170E
180
170W
160W
L1
M1
M2
L2
M3
M4
280
270
260
250
240
230
220
210
200

Fig 5

Z = 1 km Streamlines & Zonal Flow Speed

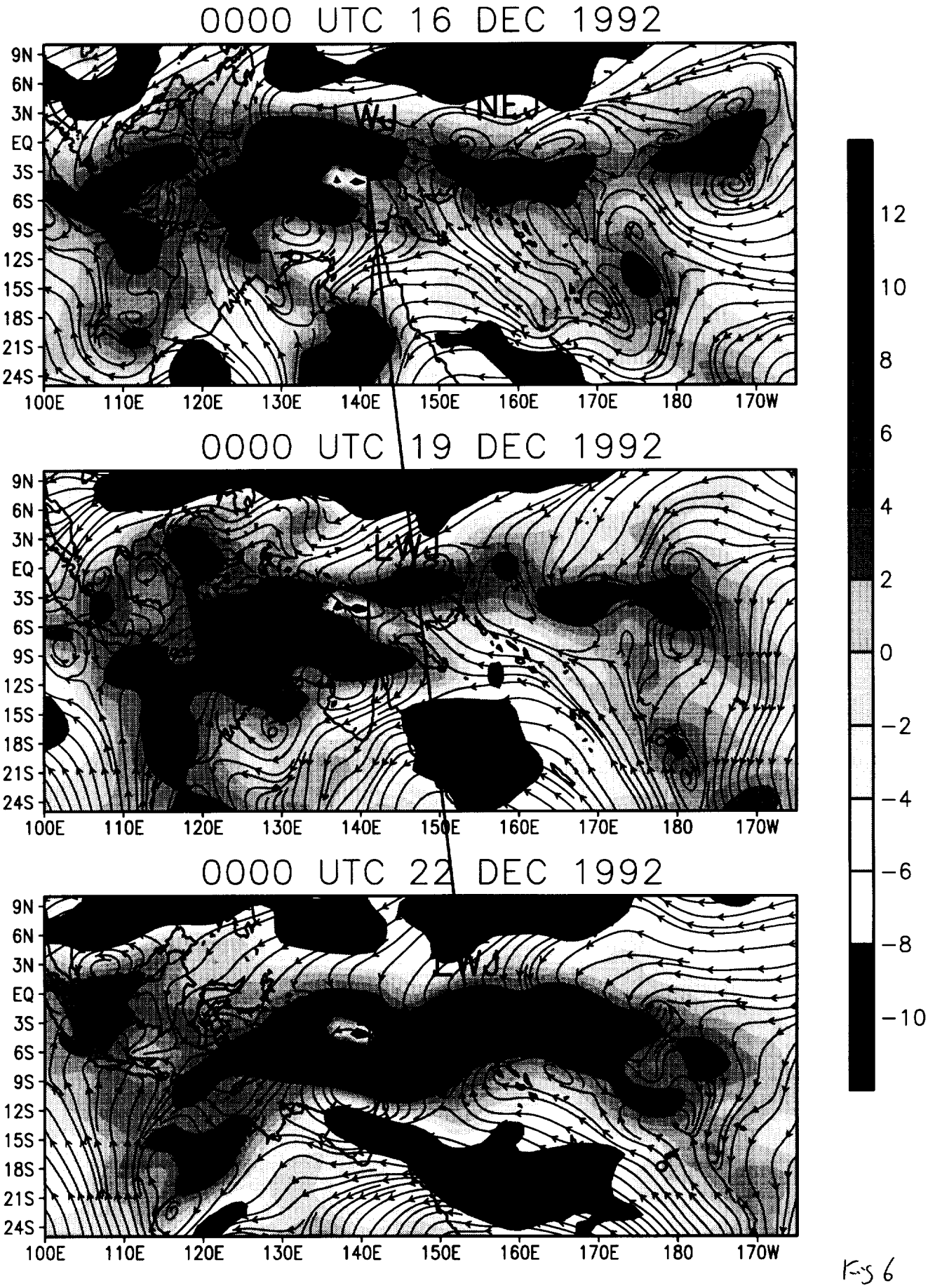

Fig 6

Z = 1 km Vorticity & Streamlines

0000 UTC 16 DEC 1992

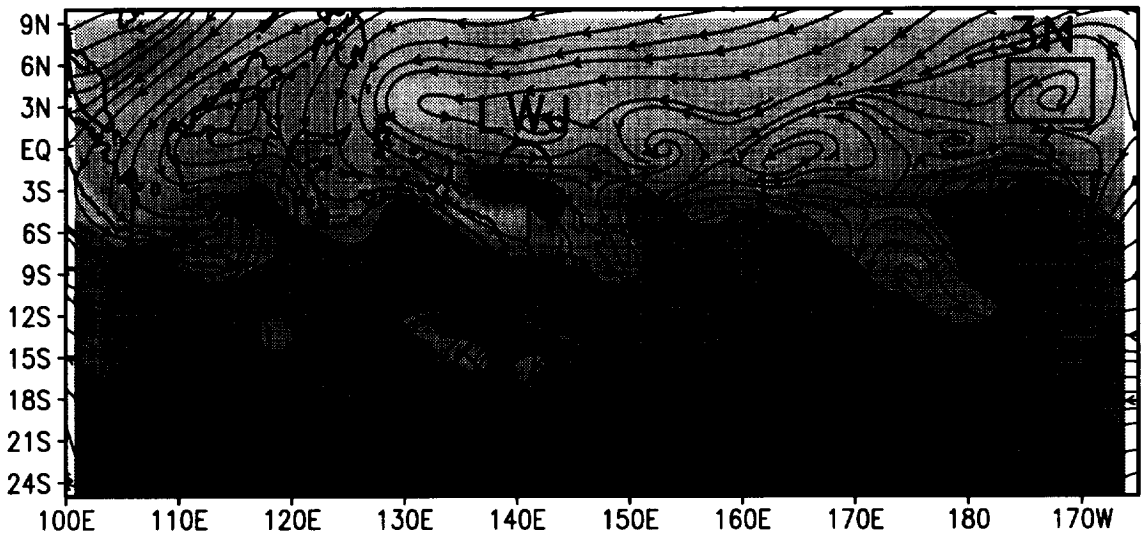

0000 UTC 19 DEC 1992

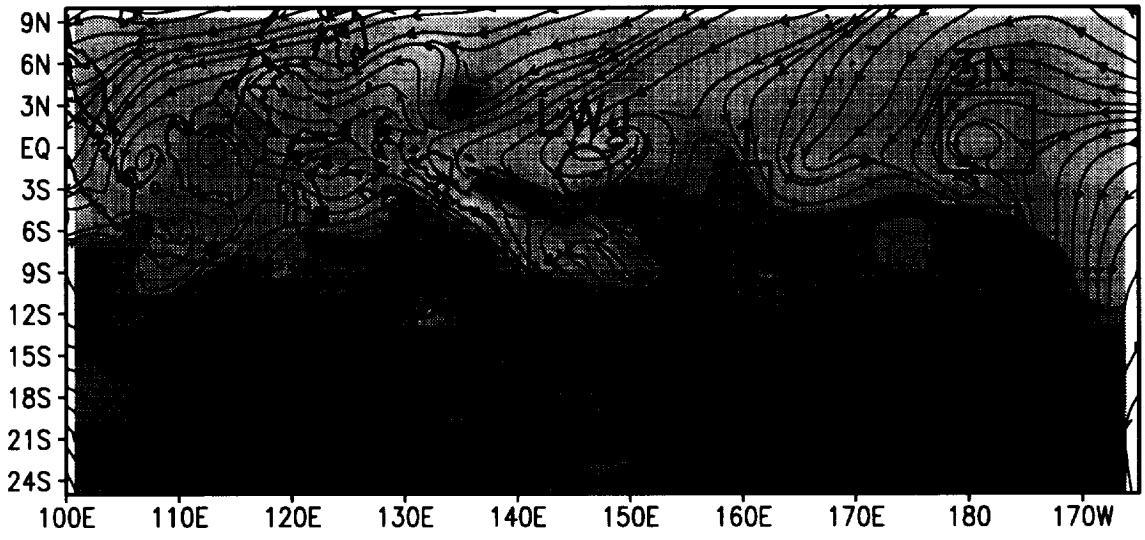

0000 UTC 22 DEC 1992

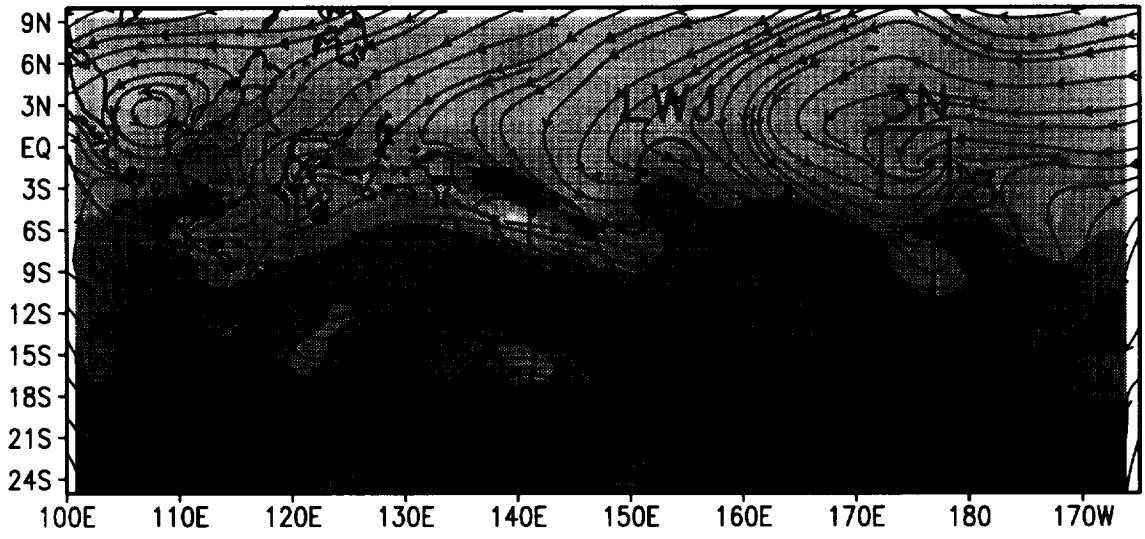

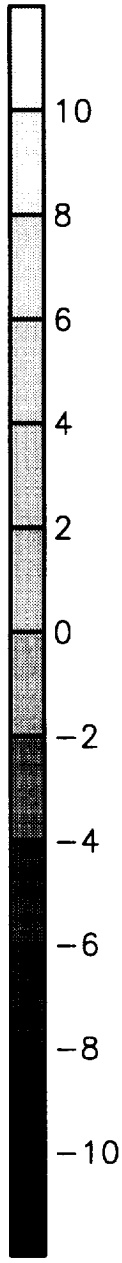

F57

Z = 1 km Streamlines & GMS Tbb

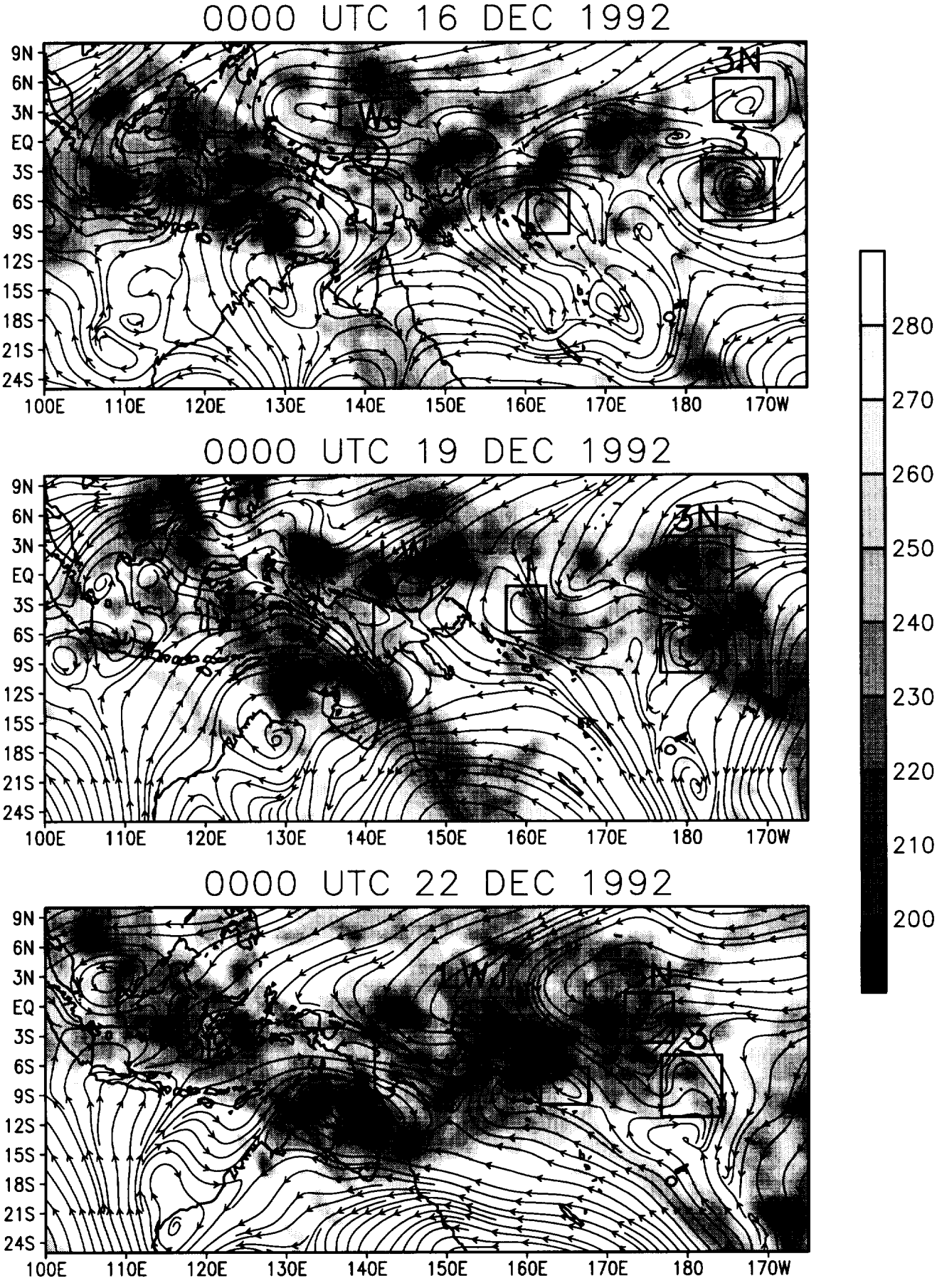

Fig 8

Z = 1 km Streamlines & GMS Tbb

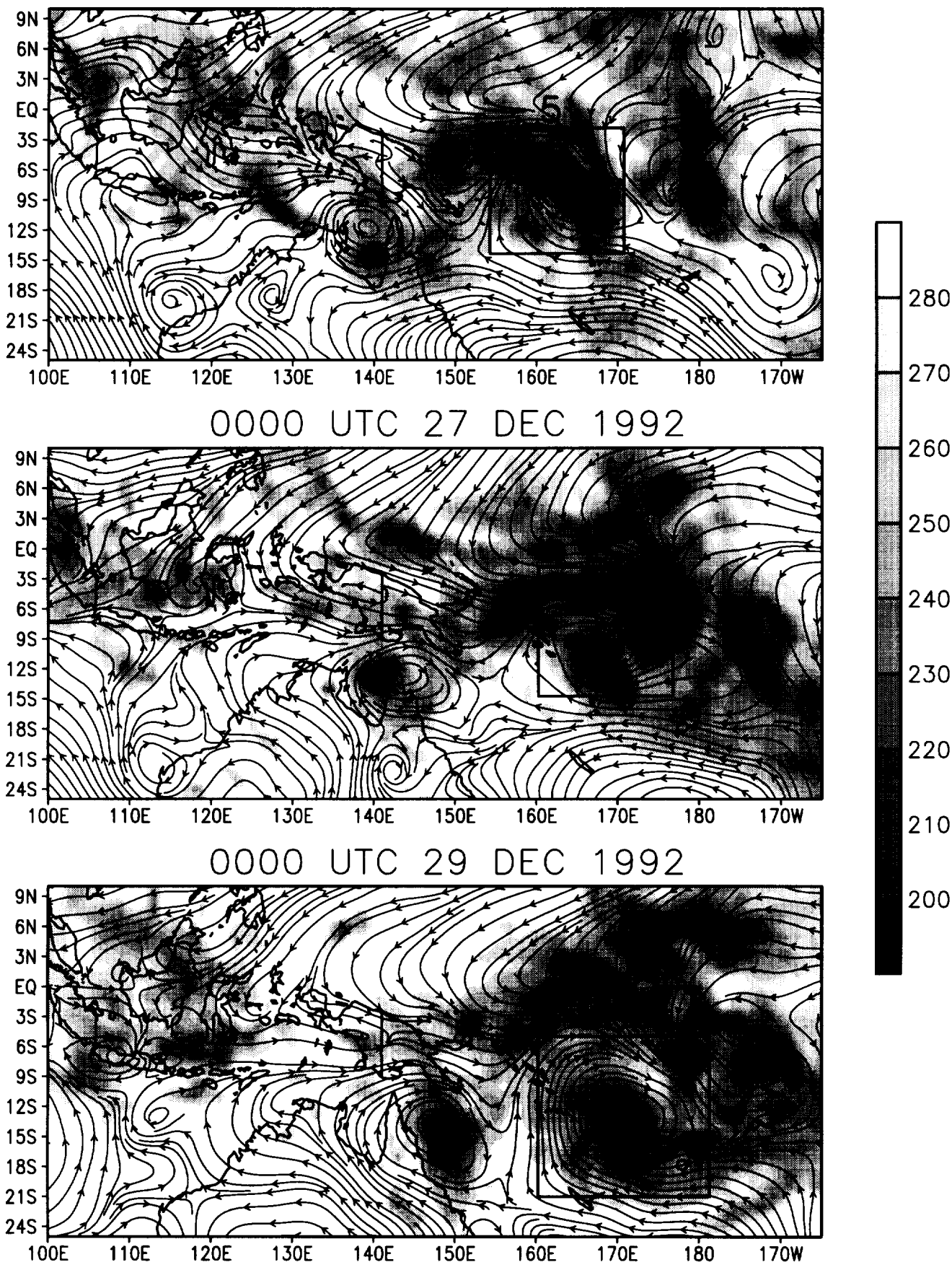

F-S 9

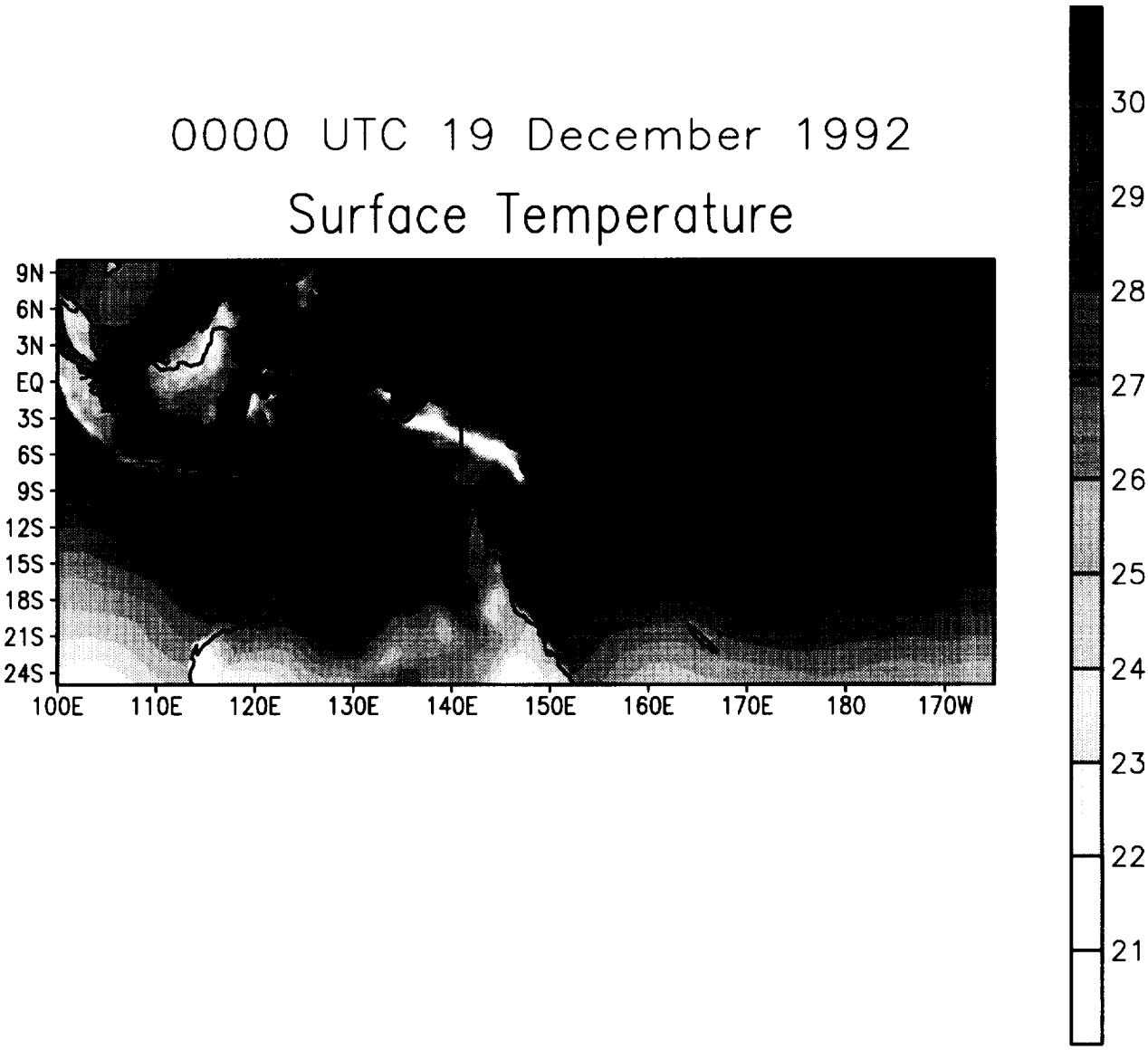
0000 UTC 19 December 1992
Surface Temperature
9N
6N
3N
EQ
3S
6S
9S
12S
15S
18S
21S
24S
100E
110E
120E
130E
140E
150E
160E
170E
180
170W
30
29
28
27
26
25
24
23
22
21

Fig 10

Z = 1 km Streamlines & Zonal Flow Speed

0000 UTC 25 DEC 1992

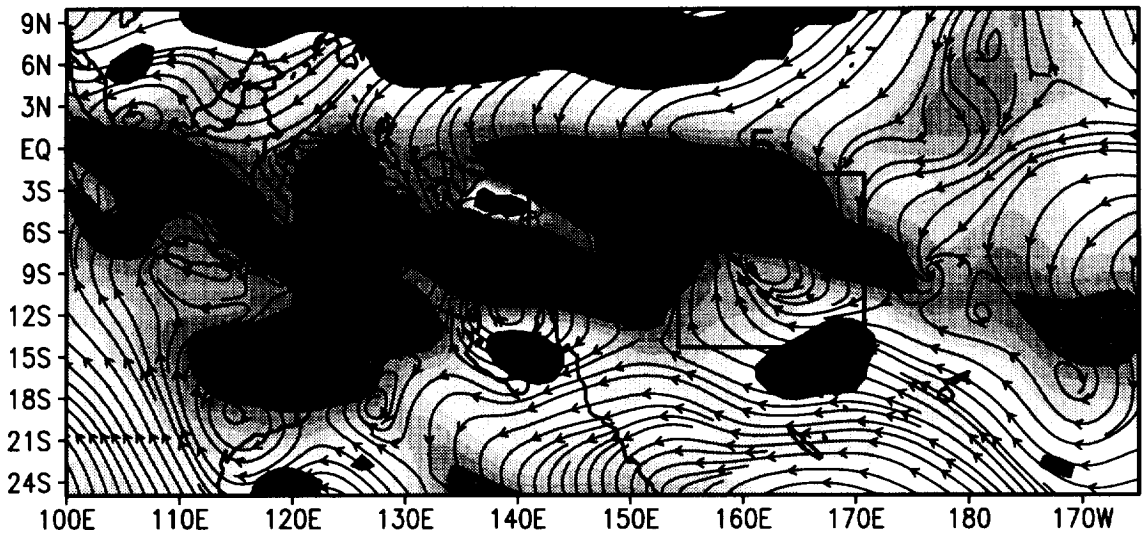

0000 UTC 27 DEC 1992

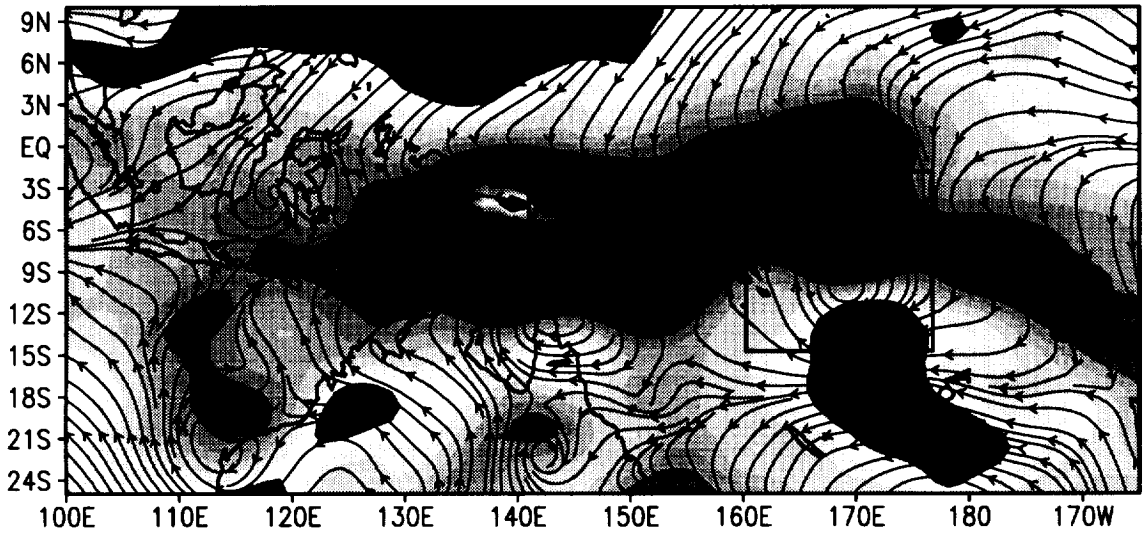

0000 UTC 29 DEC 1992

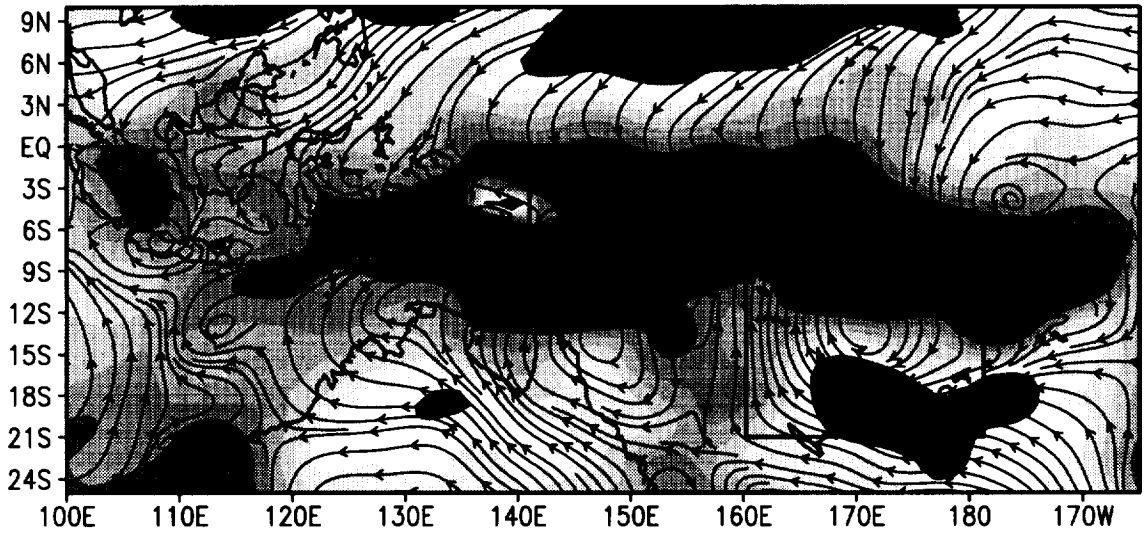

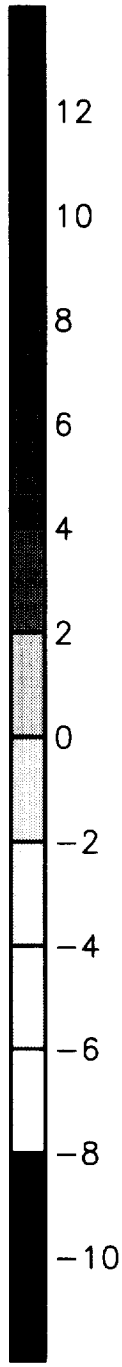

FSU

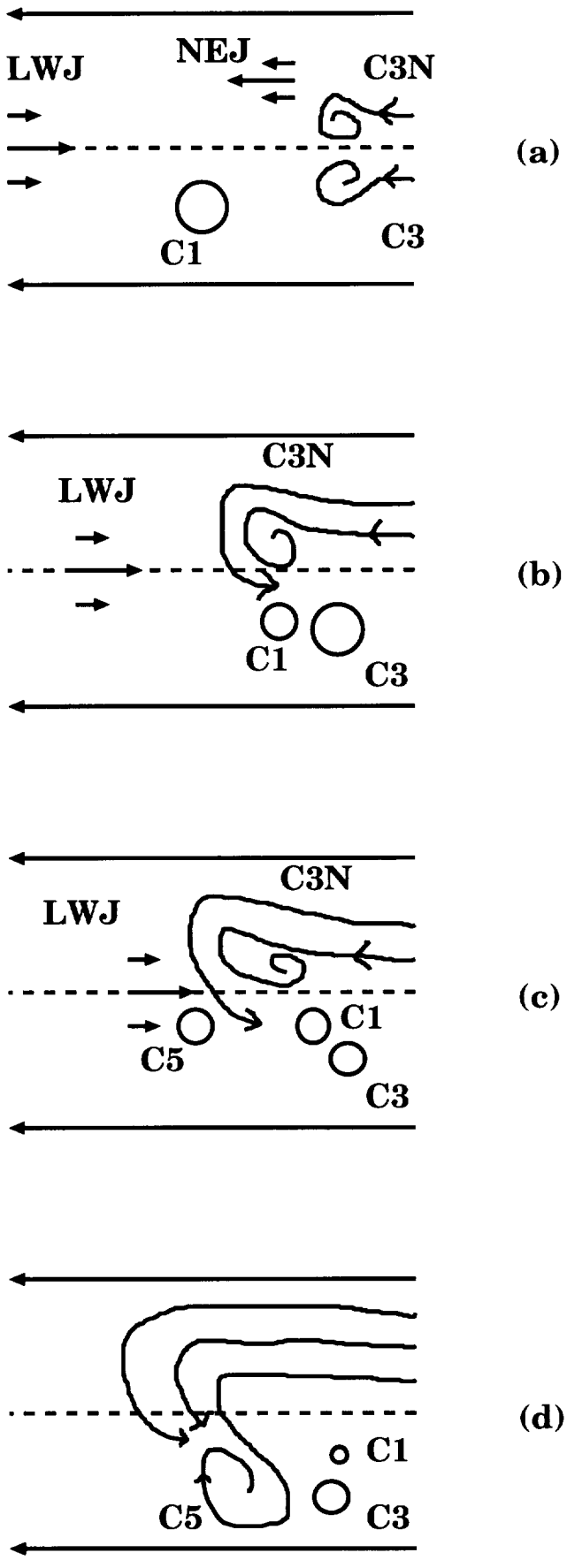

Fig 12

Z = 1 km Vorticity & Streamlines

0000 UTC 20 DEC 1992

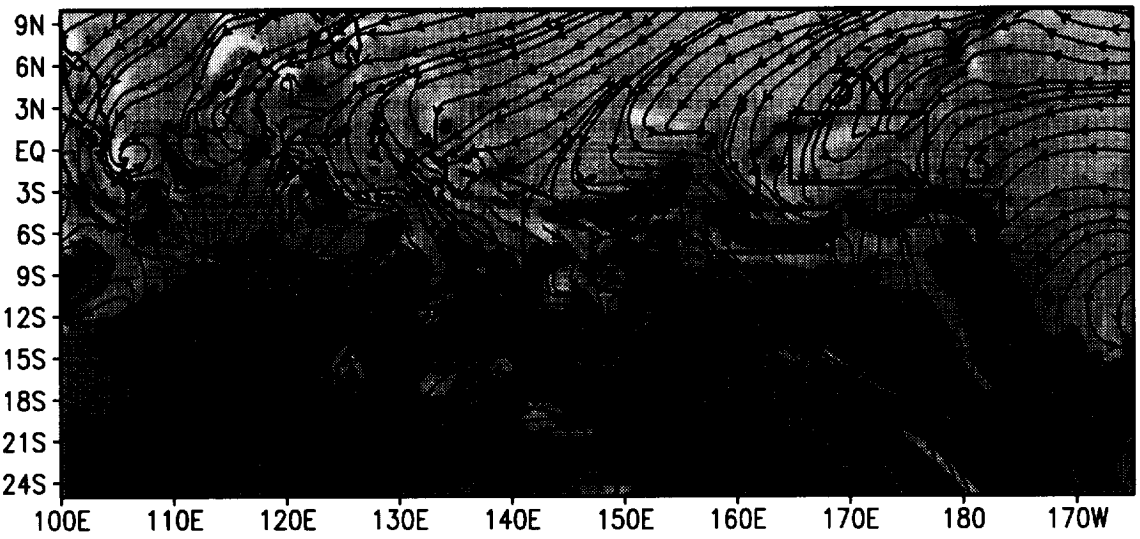

0000 UTC 22 DEC 1992

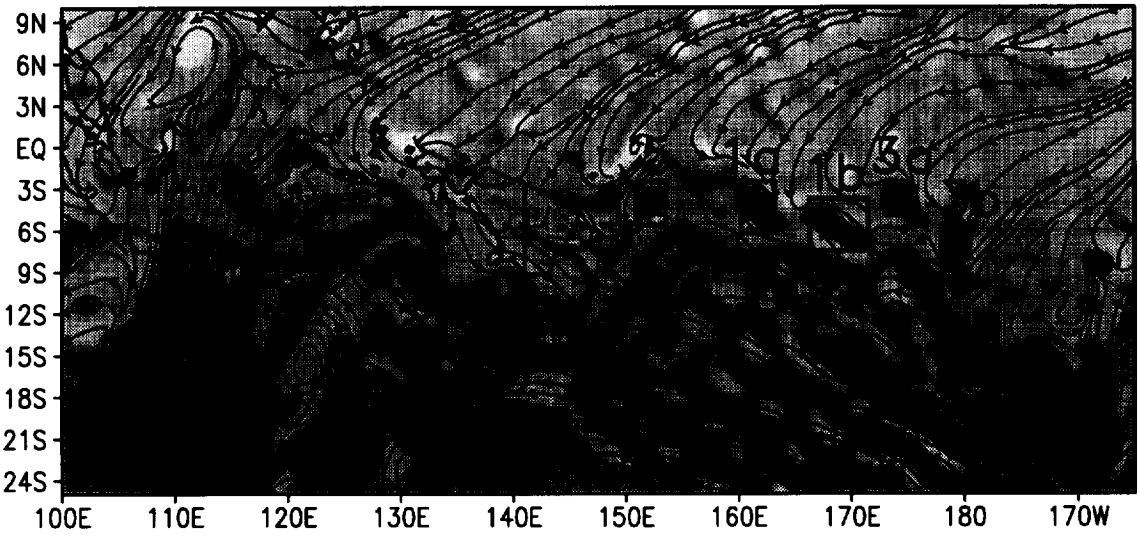

0000 UTC 24 DEC 1992

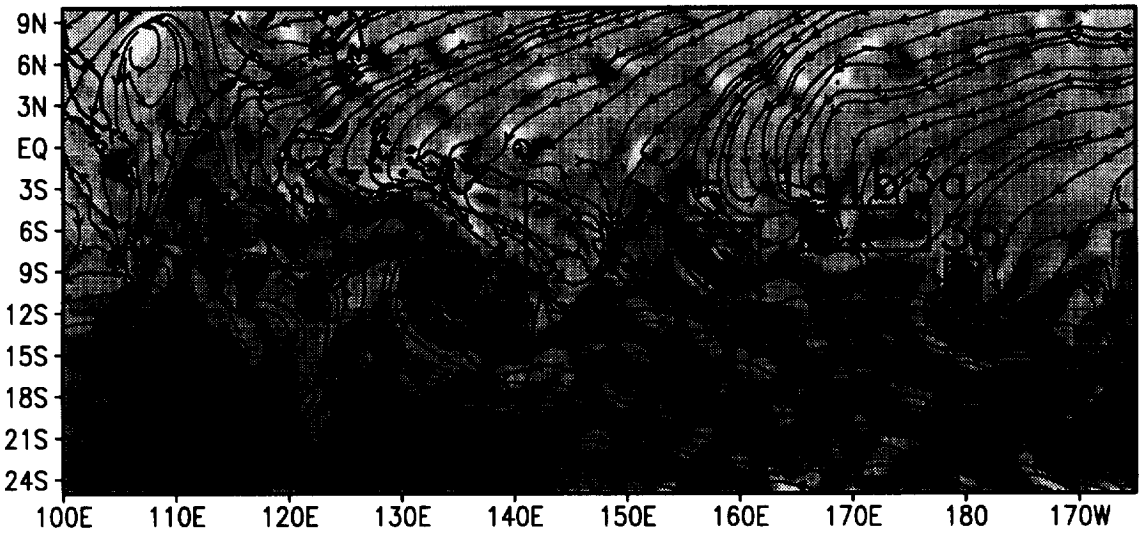

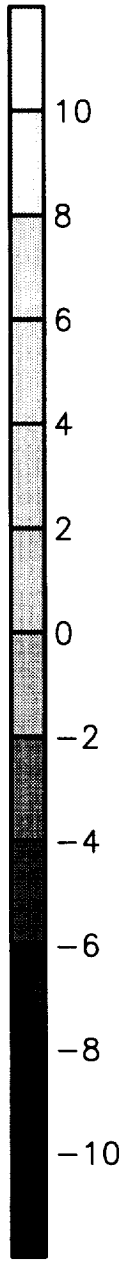

F-13

Z = 1 km Vorticity & Streamlines

0000 UTC 25 DEC 1992

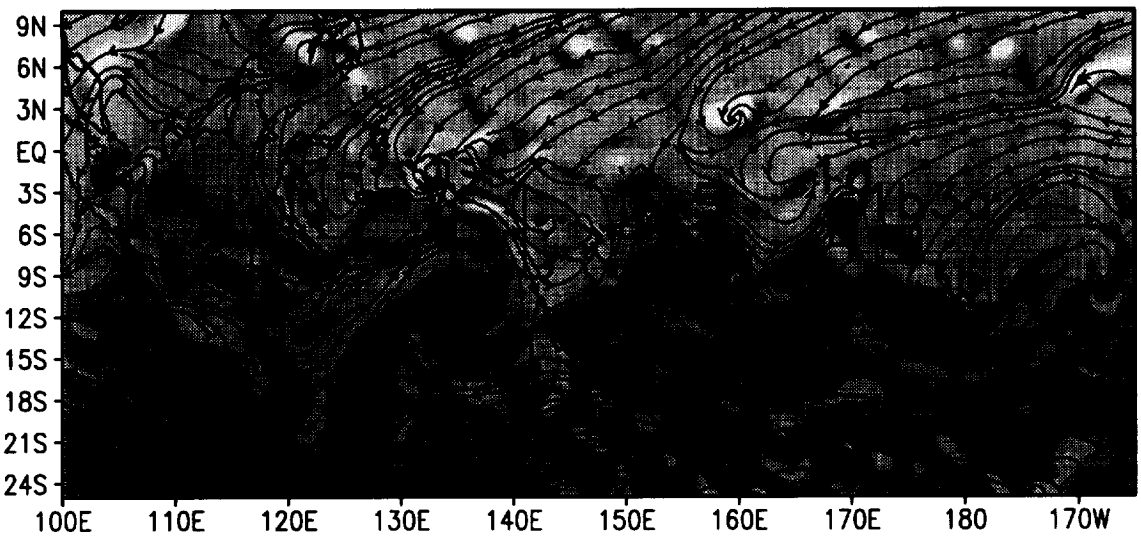

0000 UTC 27 DEC 1992

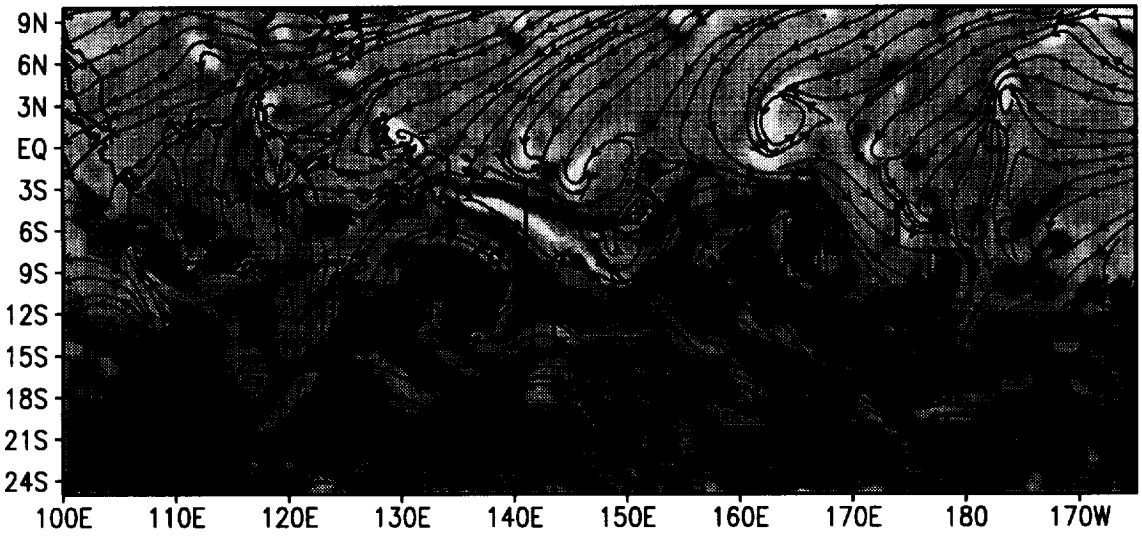

0000 UTC 29 DEC 1992

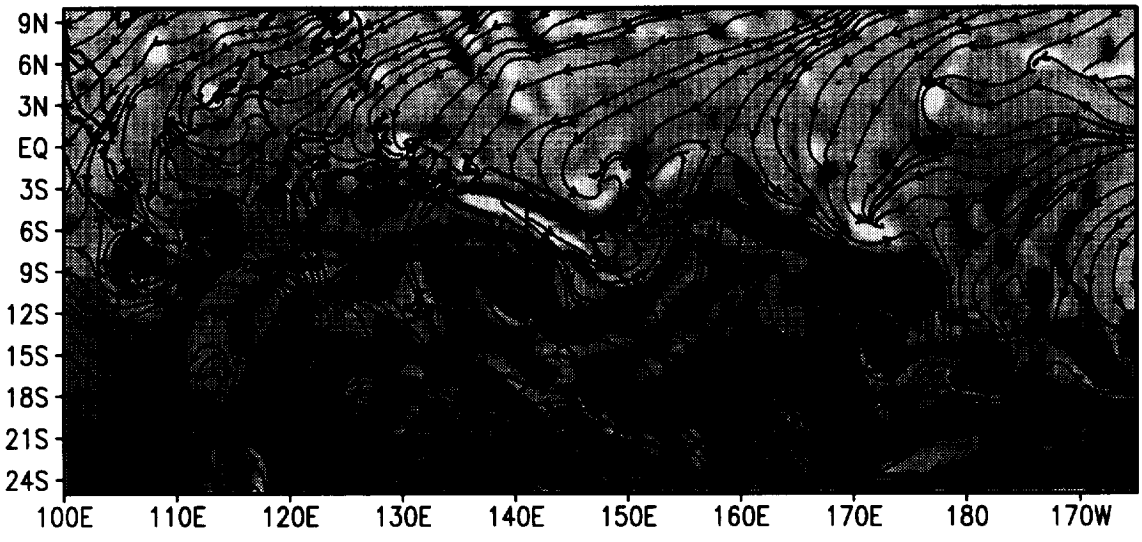

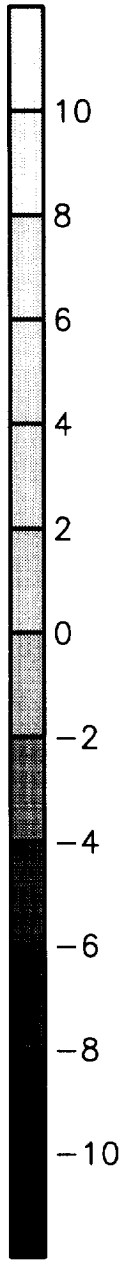

Fig 13 (cont)

Z = 1 km Streamlines & Zonal Flow Speed

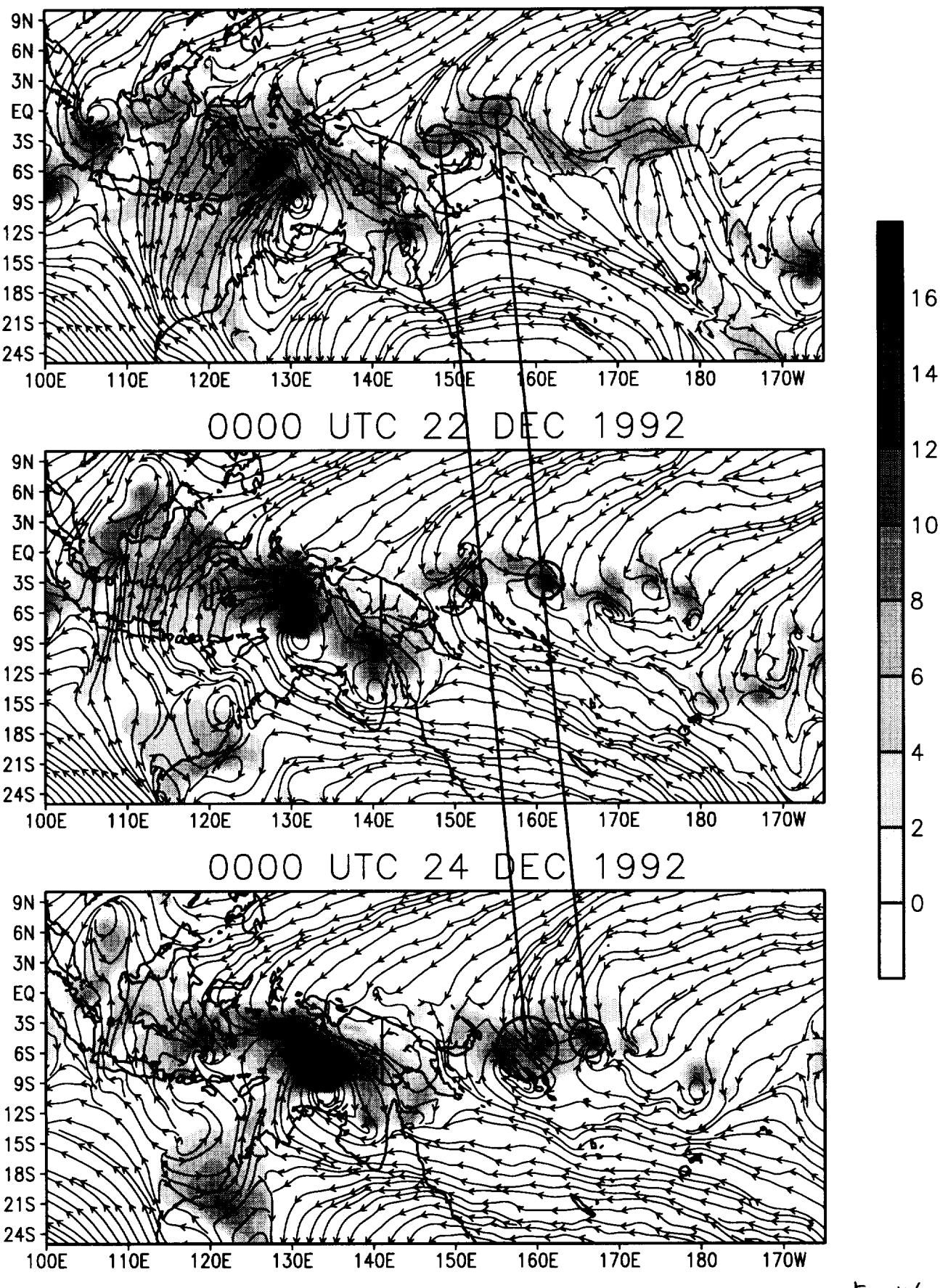

Fig 14

Z = 1 km Streamlines & Zonal Flow Speed

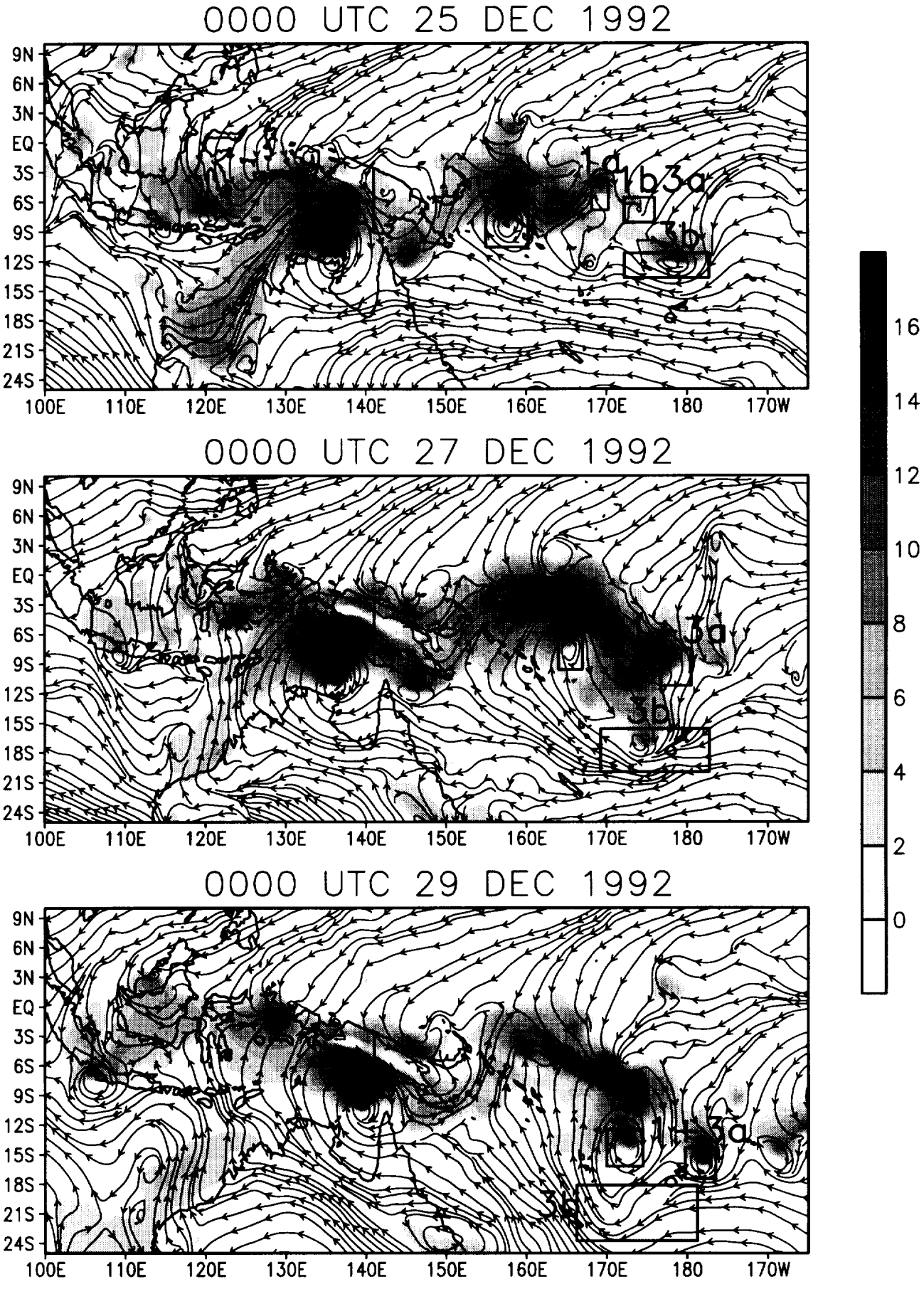

Fig 14 (cont)

24 HRS ACCU. Rain & Z = 1 km Streamlines

0000 UTC 20 DEC 1992

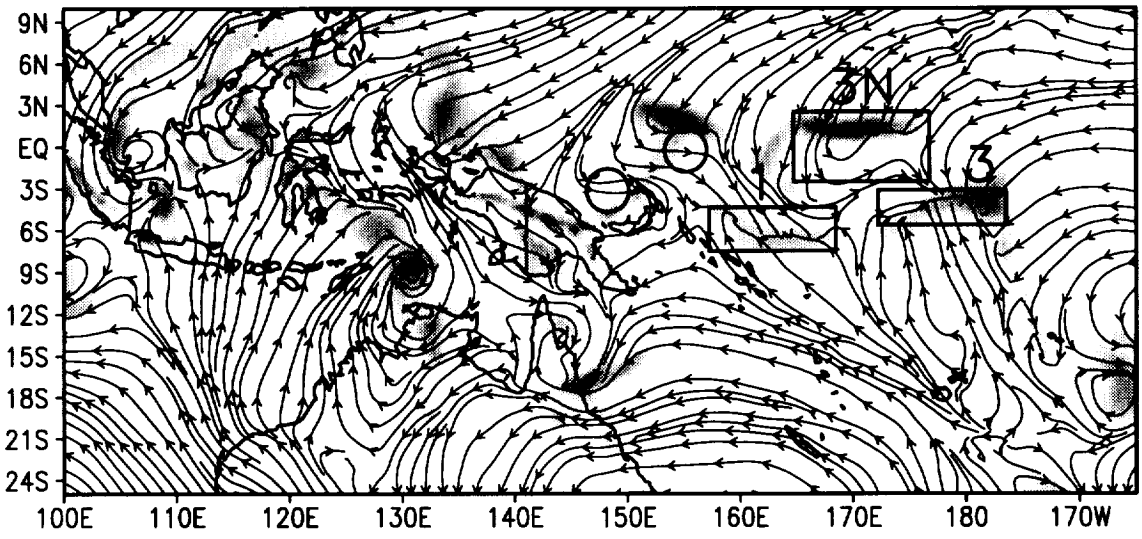

0000 UTC 22 DEC 1992

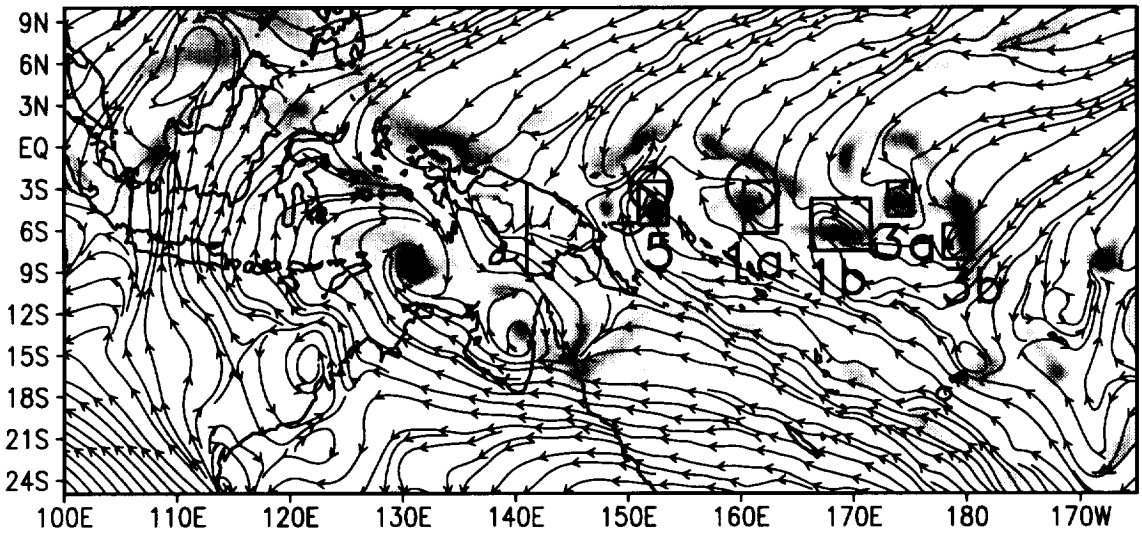

0000 UTC 24 DEC 1992

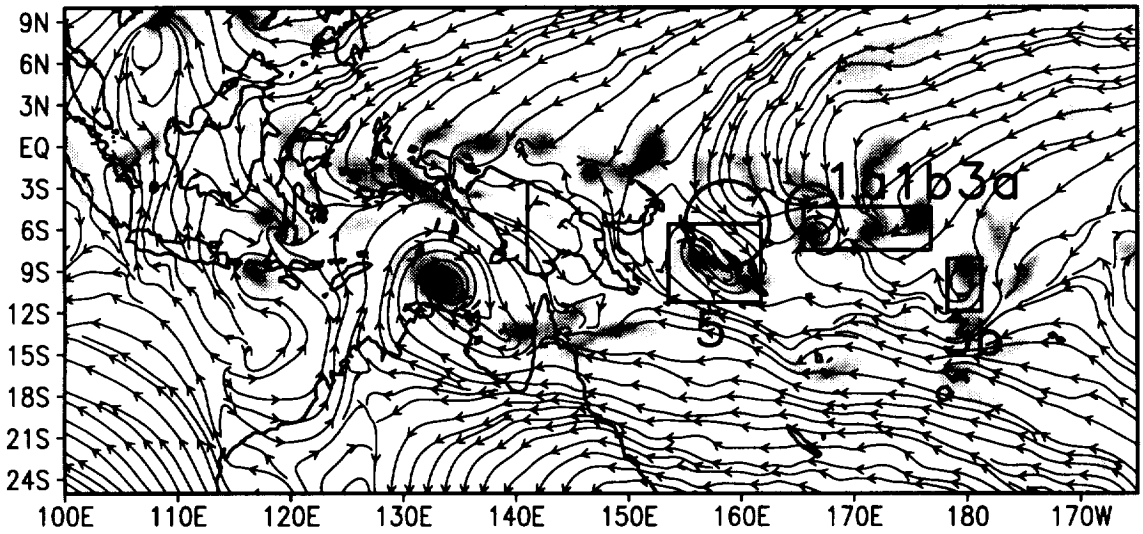

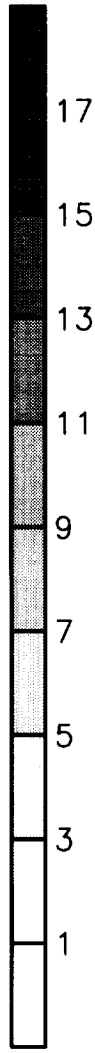

F-515

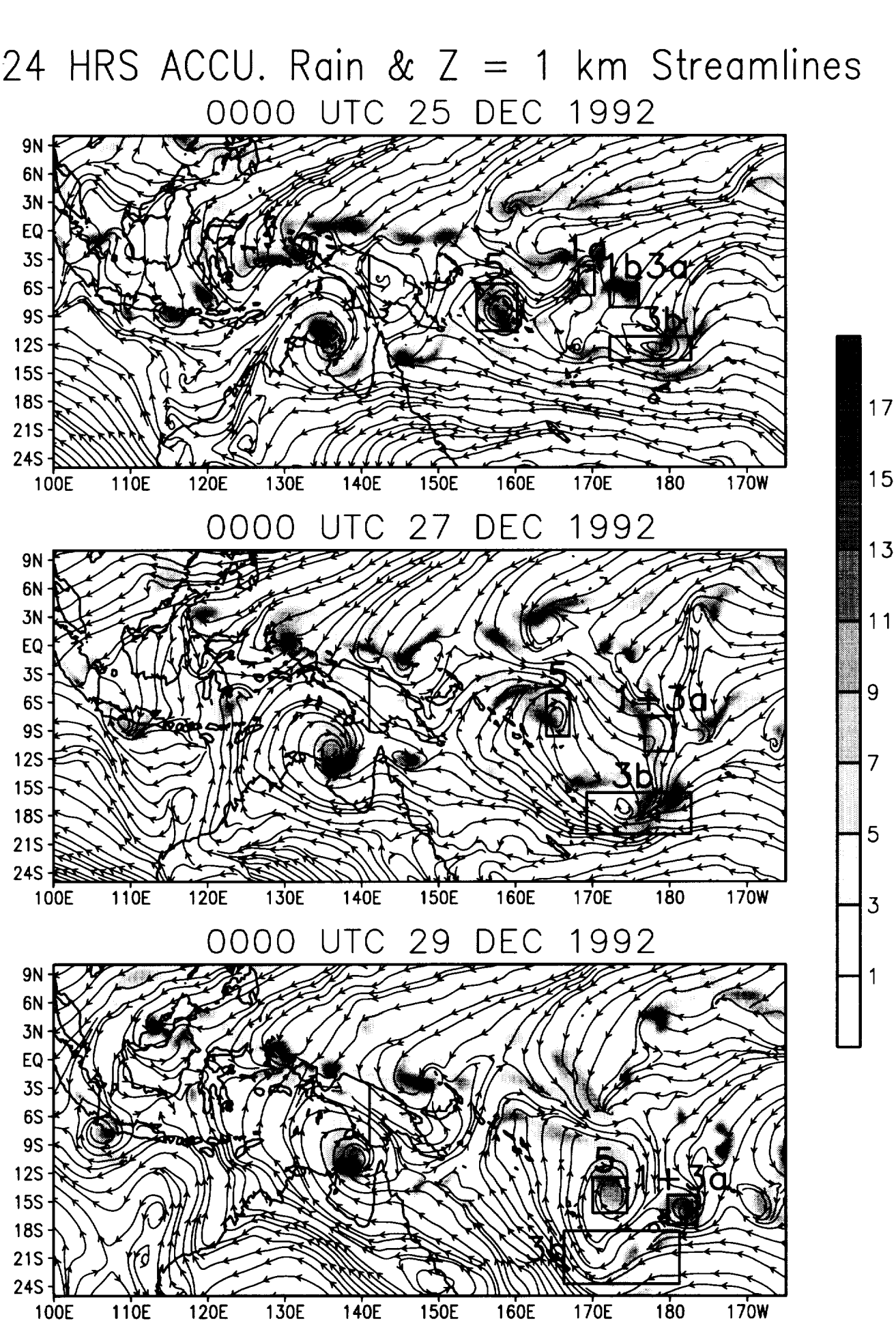
24 HRS ACCU. Rain & Z = 1 km Streamlines
0000 UTC 25 DEC 1992
0000 UTC 27 DEC 1992
0000 UTC 29 DEC 1992
9N
6N
3N
EQ
3S
6S
9S
12S
15S
18S
21S
24S
100E
110E
120E
130E
140E
150E
160E
170E
180
170W
1
1b
3a
3b
5
17
15
13
11
9
7
5
3
1

Fig 15 (cont)

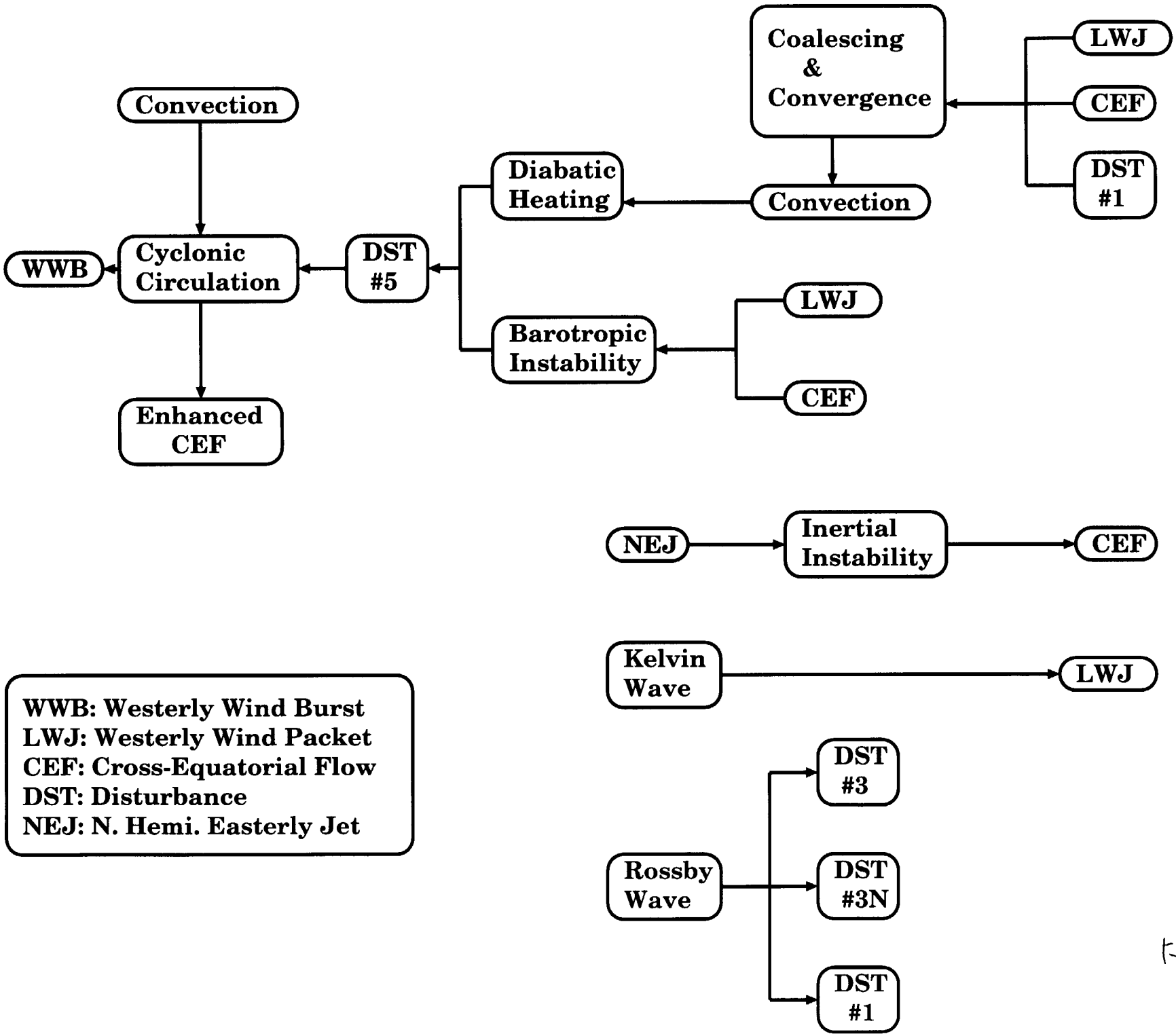
Coalescing & Convergence
LWJ
CEF
DST #1
Convection
Diabatic Heating
Convection
DST #5
Cyclonic Circulation
WWB
Barotropic Instability
LWJ
CEF
Enhanced CEF
NEJ
Inertial Instability
CEF
Kelvin Wave
LWJ
Rossby Wave
DST #3
DST #3N
DST #1
WWB: Westerly Wind Burst
LWJ: Westerly Wind Packet
CEF: Cross-Equatorial Flow
DST: Disturbance
NEJ: N. Hemi. Easterly Jet

Fig 16